

Dynamic Stability of Axially Loaded Beams on Elastic Foundations

by

Biralkumar Patel

A thesis
submitted to Faculty of Graduate Studies
in partial fulfillment of the requirements for the

Degree of Masters of Science
in

Civil Engineering

Supervisor

Dr. Jian Deng

Associate Professor - Dept. of Civil Engineering

Lakehead University

Thunder Bay, ON

June 2019

©Biralkumar Patel, 2019

Authors Declaration

I hereby declare that I am the sole author of this thesis. This is a true copy of the thesis, including any required final revisions, as accepted by my examiners. I understand that my thesis may be made electronically available to the public.

Abstract

Beams on elastic foundations have received great attention of researchers for its importance in civil engineering. The present work can be applied, for example, to the study of dynamically loaded finite columns which are embedded in soil and supported by a layer of bedrock, or to the dynamic buckling analysis of longitudinal fibers in a composite elastomer.

The dynamic stability of simply supported beam-column under periodic axial loading, and laterally resting on an elastic foundation is investigated. The combined effect of stiffness and damping is exerted on the beam through the foundation.

Traditionally, the periodical sinusoidal waveforms have been considered as the axial dynamic loading. However, in practical engineering, dynamic loading may exhibit other waveforms. Therefore this thesis considers various periodical waveforms as excitations in the derivation of the dynamic stability.

The equation of motion for the system is derived. This equation is further processed and transformed into the Hill equation. The conditions for dynamic stability regions are developed using Pipes matrix method for periodical loadings. The theoretical solutions are provided for various waveforms such as rectangular loading, sawtooth loading, exponential loading and sum of the step loading. In order to conduct numerical simulations and to develop the diagram for dynamic stability region, certain reasonable assumed values are taken for mechanical property of beam and various parameters.

Using dynamic stability plots, effects of various parameters such as flexural stiffness of beam, damping, and stiffness of foundations are studied and discussed on dynamic stability of a beam. Moreover, the first three vibration modes of beam modal analysis are conducted. In order to evaluate the accuracy of the solutions, a comparison is made among the solutions obtained from Pipes matrix method, Floquet theory, and finite element method.

As an example of applications, the study of buckling of rock slope resting on the elastic foundation is carried out and is modeled for blasting vibrations. In addition to that, the factors affecting the buckling of rock slope with blasting are also discussed. The dynamic stability solutions for arbitrary loadings are illustrated using wind sampling data which is obtained.

Keywords : Dynamic stability, Pipes matrix method, beams on elastic foundations, stress waves, rock slopes.

Acknowledgements

I would firstly like to thank my thesis advisor Dr. Jian Deng. The door to Dr. Deng's office was always open whenever I ran into a trouble spot or had a question about my research or writing. He has supported me with his patience, motivation, enthusiasm, and immense knowledge. I could not have imagined having a better advisor and mentor for my Masters study.

I owe my largest debt to my family and friends for their love, affection and encouragement which helped me in completion of this work. I also want to express my sincere thanks to my fiancée Vruti for her sacrifices, and active cooperation throughout the course of my dissertation.

Finally, I extend my sincere thanks to all those who have helped me during my dissertation work and have been involved directly or indirectly in my endeavour.

Dedication

To my loving parents, Mr. Jignesh Patel who adapted my dream as his own and Mrs. Anita Patel whose endless faith made me accomplish this thesis.

Table of Contents

Abstract	i
Acknowledgements	iv
1 Introduction	1
1.1 Introduction	1
1.2 Literature review	4
1.2.1 Dynamic stability of beams	4
1.2.2 Beams on elastic foundations	9
1.2.3 Stability of rock slope	10
1.3 Outline of thesis	13
1.4 Summary	14
2 Beams on Elastic Foundations under Dynamic Loadings	15
2.1 Introduction	15
2.2 Development of equation of motion	16

2.3	Damping modification	20
2.4	Summary	22
3	Solution with Pipes Method	23
3.1	Introduction	23
3.2	Solution for displacement	23
3.3	Stability of solution	26
3.4	Rectangular loading	27
3.5	Sawtooth type loading	31
3.6	Sum of step functions	35
3.7	Exponential variation of loadings	37
3.8	Summary	38
4	Numerical Analysis	39
4.1	Dynamic stability diagram under periodic rectangular loading	39
4.1.1	Parametric study	42
4.2	Dynamic stability assessment - Sum of step loadings	47
4.3	Comparison of solutions	48
4.4	Summary	53
5	Dynamic Stability of Rock Slopes	55
5.1	Introduction	55

5.2	Geology of the rock slope	56
5.3	Stress waves from blasting	56
5.4	Methodology	58
5.5	Results and discussion	60
5.6	Summary	64
6	Dynamic Stability of Beams under Wind Loading	65
6.1	Introduction	65
6.2	Solution using Pipes method	67
6.3	Summary	72
7	Conclusions	74
7.1	Summary of thesis achievements	74
7.1.1	Assumptions and applications	75
7.2	Future scope	76
	Bibliography	76
A	Calculation Procedures	83

List of Tables

4.1	Values of matrix components	48
4.2	Value of matrix component for $\theta = 95$ rad/s, $P_d = 336500$ N . . .	51
4.3	Reference points for dynamic stability boundary	51
5.1	Geological profile (Hu and Cruden, 1993)	56
6.1	Solution components for Example - 1	69
6.2	Solution components for Example - 2	71

List of Figures

1.1	Axially loaded beam on elastic foundation	2
1.2	Rock slope stability under axial loading	12
2.1	Deflection of foundation under effect of uniform pressure	16
2.2	Column under axial loading and Free body diagram	17
3.1	Rectangular/Step axial loading	28
3.2	Sawtooth axial loading	32
3.3	Sum of step functions	36
4.1	Dynamic stability diagram for periodic rectangular loading	41
4.2	Dynamic stability diagram for periodic rectangular loading, $\gamma = 0.48$	41
4.3	Dynamic stability diagram for periodic rectangular loading, $\gamma = 0.24$	42
4.4	Dynamic stability diagrams for $k = 1, 20, 40$ kN/m ²	43
4.5	Dynamic stability diagrams for $b = 0, 100, 200$ N	44
4.6	Dynamic stability diagrams for $n = 1, 2, 3$	45

4.7	Results of beam on elastic foundation with "Floquet theory" (Engel, 1991)	45
4.8	Results HEB 200 beam using finite element method (Briseghella et al., 1998)	46
4.9	Dynamic stability diagrams for HEB 200 beam	52
4.10	Dynamic stability diagram with respect to ratio of frequencies (γ)	52
4.11	Comparison of solutions with Floquet theory, finite element method and Pipes Method	53
5.1	Rock slope under axial loading and free body diagram	58
5.2	Dynamic buckling diagram of rock slope on elastic foundations	61
5.3	Dynamic buckling diagram of rock slope for blast loading	63
5.4	Blast loading at R = 30 m, 25 m, 20 m, 15 m.	63
6.1	Wind sampling data	66
6.2	Modified wind sampling data	67
6.3	Wind sampling data, N=30	68
A.1	Calculation sheet for pulsating force	83
A.2	Calculation sheet for Sum of step loading	84
A.3	Calculation sheet for arbitrary loading	85

Chapter 1

Introduction

1.1 Introduction

In civil engineering, beams on elastic foundations are an essential topic of research due to its broad applicability. The environmental interactions of such system are complex and often represented as static and dynamic loads. The dead loads on the system that do not change their initial amplitude and direction are considered as static loads. However, dynamic loads in realistic situations are time-dependent and may change their amplitude and direction. The analysis of beam-column resting on elastic foundation under time-varying parametric axial loads are vital, and such problems can be categorized as dynamic stability problems. Research for such subject was accelerated in the mid of 20th century when researchers learned how crucial it is to understand the behavior of beam-column under dynamic loadings in order to design and accurately analyze the stability of structural elements and also to prevent stability related collapses. Bittanti and Pastrizio (2009) explained stability analysis of the time-varying linear system, which is a study of the behavior of free motion as a function of initial state. The system is said to be stable if free vibration vanishes for any initial condition. Therefore, the dynamically stable system refers to the system which generates bounded

displacement with increasing time under the action of dynamic loading.

Such dynamic stability problems may be encountered in bridge columns (Arduino et al., 2017), submerged tunnels, pile foundations (Sun et al., 2011), railway tracks, large floating buildings, etc., these are the perfect examples of the beams resting on elastic foundations. This research focuses explicitly on cases such as vertically loaded pile foundation surrounded by soil and resting on bed-rock. This study can also be applied to rock slope stability, homogeneous rock tunnel roof and tunnel side walls where the resilience of the adjoining portions of a continuous elastic structure supplies the elastic foundation for the beam. Interactions between beam and foundation mainly depend upon the types of foundation which are categorized as Winkler, Pasternak, and Hetenyi (Engel, 1991). Understanding of static behavior of these types of foundations is the key to solve the dynamic behavior problems, and it is vital to study the impact of surrounding medium on dynamic stability and how this system will behave under various types of time-varying loadings. The general idea of an axially loaded beam on an elastic foundation is shown in Fig. 1.1.

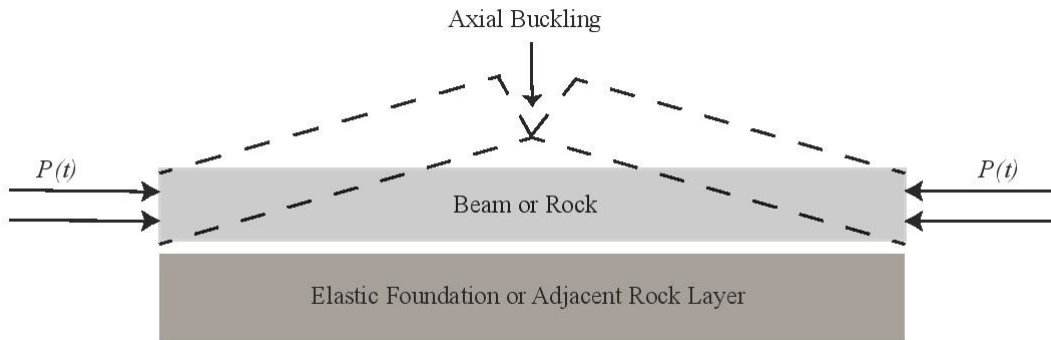


Figure 1.1: Axially loaded beam on elastic foundation

Dynamic stability study includes establishing the regions in the parameter space in which the system becomes unstable, which is called dynamic instability regions. The stable and unstable regions are separated by dynamic stability boundaries.

These boundaries are drawn in a parameter space that includes dynamic load amplitude, excitation frequency, and static load component. These diagrams are called as stability diagrams. Dynamic stability for beams on elastic foundations is usually derived from a second order homogeneous equation. The pattern of loading is usually adopted for dynamic stability study in the form of periodic sinusoidal function (Bolotin, 1964; Briseghella et al., 1998; Engel, 1991), but the true nature of applied load can be of any waveform and can also be arbitrary or even random (Huang et al., 2017). So it becomes critical to derive dynamic stability problems of various waveforms, including the arbitrary periodic waveforms.

So far, literature is oriented for investigation of the beams on the elastic foundations for various end conditions, beam properties, foundation properties, and stability methods. However, all literature has considered a periodic sinusoidal waveform as excitation. In the environment, excitation can be of almost any type, so it is vital to investigate various other periodic waveforms such as sawtooth, step loading, exponential loading, and any arbitrary loading. That leads us to our objective of investigation of the beams on elastic foundations for various waveform excitations.

The objectives of this research are as follows:

- Analysis of dynamic stability of axially loaded beams laterally resting on the elastic foundations for various types of loading patterns with Pipes matrix method (Pipes and Harvill, 2014).
- To conduct a parametric study over the system and also incorporate plotting of dynamic stability regions for various mode shapes.
- To compare results obtained from the Pipes method with the finite element method.

- Assessment of dynamic stability of rock slope against the blast vibration.
- Investigation of the dynamic stability of the beams under wind excitation.

Among many methods such as Floquet theory (Bolotin, 1964), finite element method (Briseghella et al., 1998), and Pipes matrix method (Pipes and Harvill, 2014), for separating stable bounded displacement solutions and unstable unbounded displacement solutions, Pipes method has the potential to solve the linear system not only for periodic defined functions but also for arbitrary functions. Numerical experimentation and calculated examples are also presented to illustrate the process of dynamic stability analysis thoroughly. Moreover, dynamic stability regions for certain cases have also been presented and explained.

1.2 Literature review

Dynamic stability study for beams on elastic foundations starts with formulating governing equation of motion for the system. This equation of motion usually is reduced to Mathieu - Hill equation that can be solved by analytical, numerical and experimental methods like Bolotin proposed method (based on Floquets theory), Galerkin's method, Lyapunov second method, as well as pipes matrix method. As an important application, the stability of rock slopes will be reviewed.

1.2.1 Dynamic stability of beams

The governing equation for the dynamic stability problems is usually derived as the second order differential equation that has a variable coefficient of periodic functions. The dynamic stability of systems has no accurate solution; therefore, researchers have been investigating different approximate methods for these kinds

of problems. The main objectives are to develop the method for discovering the response of the system, and assessment of stability associated with the response.

In 1924, for the first time, the problem of dynamic stability of beams under periodic loads had been investigated by Beliaev (1924). The simply supported end condition and sinusoidal axial dynamic load were considered. Hence, Beliaev obtained Mathieu- Hill equation which became an important base for many dynamic stability-related problems. Hill equation can be presented as

$$f''(t) + a(1 - b * P(t))f(t) = 0, \quad (1.1)$$

where a is the natural frequency of system and b is the excitation parameter, $f(t)$ denotes time-dependent displacement, and $P(t)$ is a periodic longitudinal force, where if $P(t)$ is a sinusoidal function then Eq.(1.1) becomes Mathieu equation. Beliaev analysis did not include the dynamic stability study about Euler beam for various end conditions which was derived by Krylov and Bogoliubov (1935) with Galerkin method. Later, more detailed study about axially loaded column was presented by V.V. Bolotin (1964) in his book on Dynamic stability of elastic system where he had defined the critical frequency for dynamic instability and developed the first three dynamic instability regions in which the displacements of the beam under the action of continuous dynamic loading were unbounded. The loading was taken in form of $P(t) = P_0 + P_t \cos(\theta t)$, where P_0 is the static load component, P_t is the amplitude of loading and θ is the angular frequency (rad/s) of the applied loading. The dynamic instability regions were originated when ratio of excitation frequency to natural frequency is $\frac{1}{3}$, $\frac{1}{2}$, 1. Bolotin's method was based on the characteristic equation where real roots of characteristic equation coincide with the region of an unboundedly increasing solution of second order linear differential equation, whereas the region of complex characteristics roots

corresponds to the bounded solution. Bolotin's book also incorporates discussion about damping impact on dynamic stability region of a beam. Burney and Jaeger (1971) used Bolotin's method for investigating the dynamic stability of uniform column for different end conditions where the column was divided into different segments and assumption was made that each segment is massless spring with lumped masses. Bolotins method was also used for studying the parametric instability of thin-walled composite beam (Machado et al., 2007).

Pipes (1953) developed a matrix based method to solve the general second order differential equation based on dividing the excitation period T into n fundamental intervals so that $T = nt$, where the first matrix solution for the initial case, i.e., the time is zero, can be constructed, and then consecutive matrices can be built at intervals t . Dynamic stability conditions can be obtained from matrix multiplication of all interval matrices. The dynamic stability boundaries separate unstable vibrations with the stable ones. Other work of Pipes' includes the dynamic stability of a uniform straight column excited by pulsating load (Pipes, 1964), where the author considered pinned-pinned column subjected to loading whose time graph is square, the regions of instabilities with the matrix algebra method were attained. More general end conditions such as clamped-clamped were also investigated for pulsating forces.

Brown et al. (1968) illustrated a method of solution for dynamic instability problem by the finite element method for bars of various end conditions, and to draw a conclusion as to the nature of the regions of instability and their dependence on modes of free vibration and static buckling. Further advancement in finite element method (FEM) for dynamic stability problems were carried out by Abbas (1978). The author developed a new finite element model to investigate the effect of shear deformation and rotary inertia on natural frequency and also on the region of dynamic instability. In addition to that, the effects of elastic foundation

on the natural frequency, static buckling loads and region of dynamic instability were examined. Abbas also incorporated the dynamic stability analysis of three-dimensional frames subjected to various loading conditions using FEM. Shastry and Rao (1987a; 1987b) established dynamic stability boundaries for an intermediate periodic concentrated load for various load positions acting on cantilever column.

Briseghella et al. (1998) derived region of dynamic stability for beams and also for frames. The method was developed for analyzing the behavior of structures of any shape such as shallow shells and curved beams. Impact of elastic foundation on dynamic stability region of a beam was also integrated. In order to evaluate the accuracy of finite element approach, a set of numerical experimentation was conducted, where dynamic stability diagram was developed for HEB 200 beam and was compared well with theoretical solutions with a practically negligible difference. Apart from that Mohanty (2007) used finite element method to study the effect of localized damage on the dynamic stability of a pre-twisted cantilever beam. The study mainly focused on phenomenon of parametric resonance. When the foreign excitations are parametric with respect to a specific form of deflection of the beam-column, they appear as one of the coefficients in the homogeneous governing equation of motion of the system. Such systems are said to be parametrically excited, and the associated instability of the system is called parametric resonance. Mohanty et. al. also examined functionally graded Timoshenko beam for its static and dynamic stability (Mohanty et al., 2011, 2012).

In general, relatively few experimental studies have been conducted in the field of dynamic stability of the beam. Bolotin (1964) presented very first experimental study. The simply supported flat-steel bar under parametric excitation was experimented to validate the results of dynamic stability regions as well as the response of flat steel bar. In the region of dynamic instability, the transverse

vibration of beam increases in high amplitude and growth of traverse vibration initially follows the exponential law of response which is the same as that in analytical results. Similar experimental work was conducted with beam specimen as Polymethyl Methacrylate known as Plexiglass or Acrylic glass (Stevens and Evan-Iwanowski, 1969). They experimentally investigated dynamic stability behavior of the viscoelastic material column under parametric excitation and found reasonable agreement with analytical findings.

The effect of fixed-fixed and fixed-pinned end conditions of the column for dynamic stability was studied and experimentally verified (Iwastubo et al., 1973). They used a finite difference method for dynamic stability analysis.

Svensson (1996) experimentally studied the dynamic buckling and dynamic stability of a beam with transverse constraints, where the adjustable flat stoppers were used to restrain the beam vibrations till specific displacement. Moreover, a model for the impact of the beam and constraints was proposed, as impact conditions at constraints were of crucial importance. Furthermore, the author investigated damping effects of the periodically loaded non-linear dynamic system, where Floquet theory and finite element method were used to include not only material damping but also to incorporate damping effects at beam hinge (Svensson, 2001). In order to capture beam material damping, a glass-mat-reinforced thermoplastic material was chosen. Svensson concluded that in order to get the most accurate damping estimation, it is vital to consider two dampings separately, one from the hinges of the end supports and second from the beam material itself.

Mohanty (2007) experimentally investigated parametric resonance of beams with localized damage, sandwich beams and pre-twisted cantilever beams with localized damage for dynamic instabilities. In addition, fixed-free, pinned-pinned, fixed-fixed and fixed-pinned end conditions were considered. Aluminum strips

were used as an experimental specimen, where rectangular cut-outs of suitable dimension were made at essential places to yield the effect of specified artificial damage. The cut-outs were filled with an epoxy compound (M-seal), whereas sandwich beam specimens were composed of steel sheets as cover and P.V.C. as a viscoelastic core. The experiments of the beam with localized damage and sandwich beam for fixed-free and fixed-fixed end conditions were in close agreement with the theoretical results, whereas deviation in results was encountered in case of pinned-pinned and pinned-fixed cases since damping presence in hinges was not considered in theories.

1.2.2 Beams on elastic foundations

Extensive studies on beams and plates resting on the elastic foundation have been done. These studies mainly categorize as numerical and analytical approaches. Dynamic stability of beams having variable cross-sections supported on an elastic foundation was first studied by Ahuja and Duffield (1975) both theoretically and experimentally, where they investigated the effect of the beam with linear variable cross-section on dynamic stability regions and concluded that under the effect of the elastic foundation, the width of dynamic stability regions was decreased and the amplitude of parametric resonance was also reduced. Another study was presented by Eisenberger and Clastornik (1987) on the vibration of the beam on a variable Winkler foundation. They presented and compared two methods of solving the eigenvalue problem of vibration and stability of a beam on an elastic foundation.

Similarly, Abbas and Thomas (1978) studied Timoshenko beam on the elastic foundation for sinusoidal excitation and considered various end conditions. Moreover, they also developed dynamic stability regions for the first five modes of vibration where the width of dynamic stability regions increases with the mode

number of vibration. Yokoyama (1988) compared results between Timoshenko beam and Euler Bernoulli beam on elastic foundations. In order to evidently illustrate the effect of elastic foundation on dynamic stability region of the beam, Yokoyama developed dynamic stability regions for beam, one with and the other without foundation. After examining the impact of static load factor, rotatory inertia, and shear deformation on dynamic stability regions, Yokoyama concluded that the increase in static load factor would move dynamic instability regions towards left in parallel along the frequency ratio axis, whereas rotatory inertia and transverse shear deformation have a destabilizing effect on the system of the beam on elastic foundation.

Engel (1991) has modified static foundation models such as Winkler, Pasternak, and Hetenyi, to incorporate damping. Stability studies were performed using Floquets method. The parametric studies were conducted to investigate the effect of foundation stiffness, foundation damping and the number of vibration modes on dynamic stability regions.

1.2.3 Stability of rock slope

Rock layer which is resting on the slope of soil (Elastic foundation) can be modeled as the dynamic stability of beams on elastic foundations. Many types of research have been submitted regarding the solution methods for the stability of the sloped rock layer resting on an elastic foundation. The study of stability of rock slope for the high-frequency wave propagation was conducted using discrete element model to assess the effects of variable frequency blasting vibrations (Dowding and Gilbert, 1988). Blasting is also one of the considerable loading types for rock slope stability. Dynamic stability analysis under blasting vibration was investigated (Chen et al., 2013). The method was based on recording the response of rock slope against different blast vibration velocities.

Tommasi et al. (2009) concluded that minor geometry variation in rock slab could initiate the instability phenomenon while water pressure is not performing a major role. Hu and Kempfert (1999) presented modeling of the buckling rock failure using a numerical method. The discontinuity behavior was introduced by joint element concepts. Moreover, they presented one sample calculation for buckling of rock slope in an open pit mining. Hu and Cruden (1993) conducted a case study on buckling of rock layer in Highwood Pass, Alberta, Canada. They classified various types of buckling in the region of Highwood pass and provided the modifications in Euler buckling method considering cohesion and safety factors.

Deng and Gu (2018) conducted research for the buckling mechanism of the pillar rockburst in underground hard rock mines under the static and blasting load. In their study, they had an innovative point of view, because they modeled the buckling of the pillar as dynamic instability, which incorporated derivation of dynamic instability for pillar rockburst using Floquet theory, and presented dynamic stability diagrams. Blasting disturbances for the pillar rockburst was modeled as periodical functions, and closed-form solutions were obtained in terms of rockburst diagrams (Deng et al., 2019).

Study about biaxially loaded rock slope buckling was conducted by Nilsen et al. (1987). They incorporated axial stress horizontal to slope face and axial stress in dip direction. The case study of Ortfjell open pit in Northern Norway based on the buckling under biaxial loading was presented. The stresses can be excited by the blasting vibration. The method is based on analyzing elastic, flexural buckling of rectangular plates, including analyzing the joints of plates. A conclusion was made that to include flexural buckling of hard rock, very special combinations of parameters such as geology, stress conditions and rock character have to exist. The configuration of the rock on slope foundation under blasting vibration is shown in Fig. 1.2.

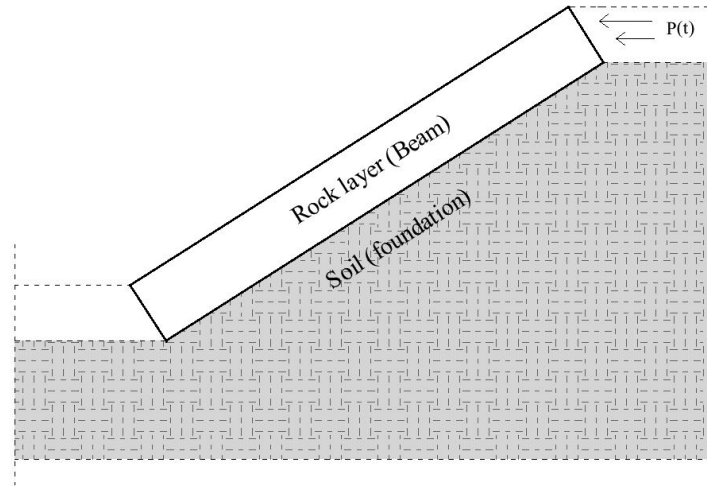


Figure 1.2: Rock slope stability under axial loading

The detailed study of failure mechanism was conducted. It states that discontinuities parallel to the surface forming slabbing causes the slip buckling slope failure. In general, the failure mechanism requires that the slope dip more steeply than the angle of internal friction along the discontinuity forming slabs involved. Three main cases of buckling involve i) flexural buckling of plane slopes, ii) three hinge-buckling of plane slopes and iii) three-hinge buckling of curved slopes(Qi et al., 2015). Various theories were used for modeling of slip buckling slope failure like Eulers formula, elastic theory, energy equilibrium principle, and finite element method. Research on the effect of stiffness and cohesion was studied on buckling failure. Earthquake is a significant cause of slip buckling slope failure, so the study was focused on the analytical solution on slip buckling slope failure considering the effect of earthquake and pore water pressure.

Buckling failure of rock slope can be originated by the following mechanism: 1) Pore pressures along the bounding discontinuity (for example, bedding). 2) Slope geometry (for example, curved, convex-up slopes). 3) Forces external to the slope which can cause unstable vibration. 4) Very high stresses in the plane of the slab (occurring, for example, on very high, continuous slabs) (Cavers, 1981). Flexural buckling is elastic buckling and follows Eulers rule which is an action of static

loading. Three hinge buckling on plane can take place due to piezometric pressure and external loading on slope causing larger displacement as a result of unstable vibrations.

1.3 Outline of thesis

This research focuses on assessing dynamic stability for axially loaded beams laterally supported on elastic foundations for various periodical loadings and also tries to establish an approach for solving the same system for arbitrary loading using Pipes matrix method (2014). A chapter wise outline is as follows.

- **Chapter 1-** Introduction, this chapter is mainly divided into two sections, introduction and literature review.
- **Chapter 2-** Beams on elastic foundations under dynamic loadings, it explains types of foundations and how they affect the system. The equation of motion for beams on elastic foundations is derived, and a detailed discussion about damping is also included.
- **Chapter 3-** Solution with Pipes method, it specifically focuses on providing the theoretical solution of Pipes matrix method for assessing dynamic stability for various types of loadings.
- **Chapter 4-** Numerical analysis, it considers the beam specimen and provides dynamic stability diagram for various cases. This chapter also includes the parametric study of the dynamic stability of beams on elastic foundations. Moreover, the comparison of the solution obtained using Pipes method with the solution obtained with Floquet theory and finite element study is presented.

- **Chapter 5-** Dynamic stability of rock slopes, the dynamic stability of the rock slopes under blasting vibrations has elaborated.
- **Chapter 6-** Dynamic stability of beams under wind loading, Wind sampling data collected from Huang et al. (2014) study is taken and processed for solving it with Pipes methods.
- **Chapter 7-** Conclusions, the conclusions drawn from previous chapters are summarized, and points for improvements in further research are suggested.

1.4 Summary

The aim and importance of the dynamic stability of beams on elastic foundations have been introduced. Various methods of deriving dynamic stability such as Floquet method, finite element method, Beliaev method, and Pipes method are discussed in brief with its applicability. Research based on beams on elastic foundations with various end conditions, different foundation conditions, and various beam models have been reviewed. This chapter also incorporates the background study about rock slope stability in various site conditions and geological conditions. Moreover, experimental researches on dynamic stability are reviewed.

Chapter 2

Beams on Elastic Foundations under Dynamic Loadings

2.1 Introduction

Beams resting on elastic foundations have been studied for considerable numbers of cases. Some of these analysis considers a single parameter for illustrating foundation behavior. In such cases, it is assumed that pressure on the foundation is proportional to the deflection of the foundation. The vertical deformation characteristics of the foundation are defined by means of identical, independent, closely spaced, discrete, and linearly elastic springs. The constant of proportionality of these springs is known as the modulus of subgrade reaction (k), which can also be defined as foundation stiffness per unit length. This simple and relatively crude mechanical representation of soil foundation was firstly introduced by Winkler (Kerr, 1964).

The Winkler model, which has been originally developed for the analysis of railroad tracks, is straightforward to take into account for mathematical modeling. However, one of the most critical deficiencies of the Winkler model is that the displacement discontinuity appears between the loaded and the unloaded part of

the foundation surface as shown in Fig. 2.1a. In reality, the soil surface does not show any discontinuity as shown in Fig. 2.1b.



(a) Winkler Type foundation

(b) practical soil foundation

Figure 2.1: Deflection of foundation under effect of uniform pressure

Here, we take the Winkler foundation model in the account for the beams on elastic foundations problem, because the solution for dynamic stability is highly complex in nature.

2.2 Development of equation of motion

The equation of motion is an equation vital to characterize the nature of a vibrating system regarding its motion as a function of time. The equation of motion can be often derived from force balance or energy balance equations of the system. Here we have used force-equilibrium to derive the equation of motion for the system, which concerns the transverse vibration of a simply supported elastic column of the uniform cross-section, laterally supported on continuous elastic foundation subjected to a dynamic axial load $P(t)$ as shown in Fig. 2.2. Prior to any loading or deflection the length of the column is taken as L .

An infinitesimal element from Euler Bernoulli beam resting on an elastic foundation is taken of length Δx with its free body diagram shown in Fig. 2.2. Taking ρ as the mass density per unit volume of the column, A be the cross-sectional area, and $v(x)$ as the transverse displacement of the central axis. Therefore inertia force (D'Alembert's force) can be given as $m\ddot{v} = (\rho A \Delta x)\ddot{v}$. The Winkler

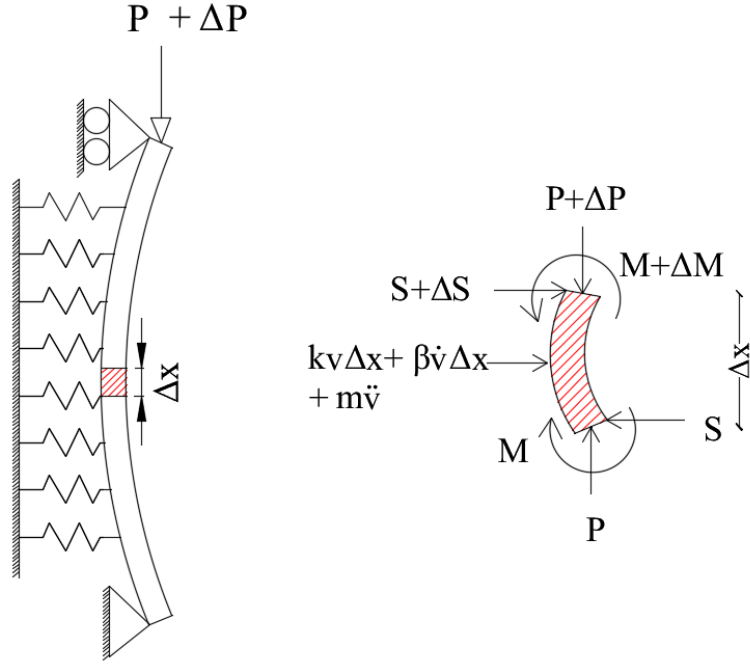


Figure 2.2: Column under axial loading and Free body diagram

type elastic foundation exerts stiffness force and damping force between beam-foundation interaction. These forces will act opposing the displacement under the axial force $P(t)$, which are shown with $kv\Delta x$ and $\beta\dot{v}\Delta x$, where k is the stiffness of the foundation per unit length and β is the damping of the foundation per unit length.

Summing up the forces in the vertical direction x yields $\Delta P = 0$, now summing up the horizontal forces v leads to

$$\Delta S + \rho A \Delta x \ddot{v} + kv\Delta x + \beta\dot{v}\Delta x = 0. \quad (2.1)$$

When $\Delta x \rightarrow 0$, Eq.(2.1) can be written as

$$\frac{\partial S}{\partial x} = -(\rho A \ddot{v} + kv + \beta\dot{v}). \quad (2.2)$$

Now summing up the bending moments at mid-point,

$$\Delta M - S\Delta x + P(t)\Delta v = 0. \quad (2.3)$$

Rearranging Eq.(2.3) results in

$$\frac{\partial M}{\partial x} = S - P(t)\frac{\partial v}{\partial x}. \quad (2.4)$$

The derivative of both sides in Eq.(2.4) gives

$$\frac{\partial^2 M}{\partial x^2} = \frac{\partial S}{\partial x} - P(t)\frac{\partial^2 v}{\partial x^2}. \quad (2.5)$$

Substituting Eq.(2.2) in Eq.(2.5) results in

$$\frac{\partial^2 M}{\partial x^2} = - \left[\rho A \frac{\partial^2 v}{\partial t^2} + kv + \beta \frac{\partial v}{\partial t} + P(t) \frac{\partial^2 v}{\partial x^2} \right]. \quad (2.6)$$

Euler Bernoulli beam follows the relationship, $M = EI(\frac{\partial^2 v}{\partial x^2})$, therefore Eq.(2.6) can be written as

$$EI \frac{\partial^4 v}{\partial x^4} + P(t) \frac{\partial^2 v}{\partial x^2} + \rho A \frac{\partial^2 v}{\partial t^2} + kv + \beta \frac{\partial v}{\partial t} = 0. \quad (2.7)$$

Eq.(2.7) is the general form of the equation of motion for an axially loaded Euler Bernoulli beam resting on Winkler type foundation. The solution to this type of equation is complex, and it can be handled through various processes. The solution in the form of displacement with respect to time is required to understand the dynamic stability behavior. Moreover, $P(t)$ can be periodic compressive or periodic tensile force. A negative value of $P(t)$ shows the tension, and positive value of the same represents the compression force.

The boundary condition for the beam is assumed to be simply supported so that displacement and bending moment on both ends are zero. Therefore,

$$\text{at } x = 0, \longrightarrow v(0, t) = 0 \ \& \ \frac{\partial^2 v(0, t)}{\partial x^2} = 0,$$

$$\text{at } x = L, \longrightarrow v(L, t) = 0 \ \& \ \frac{\partial^2 v(L, t)}{\partial x^2} = 0.$$

The solution of the equation of motion is required to be in the form of deflection with respect to time , the general solution for such case is

$$v(x, t) = \sum_{n=1}^{\infty} q_n(t) \phi_n(x), \quad \phi_n(x) = \sin\left(\frac{n\pi x}{L}\right), \quad n = 1, 2, 3, \dots \quad (2.8)$$

where $\phi_n(x)$ are the modal function of a simply supported column satisfying the boundary conditions, which possess the orthogonality property

$$\int_0^L \phi_n(x) \phi_i(x) dx = \begin{cases} 0, & \text{if } n \neq i \\ \frac{1}{2}L, & \text{if } n = i. \end{cases} \quad (2.9)$$

Substituting Eq.(2.8) into Eq.(2.7) yields

$$EI\left(\frac{n\pi}{L}\right)^4 q_n \sin\left(\frac{n\pi x}{L}\right) - P(t)\left(\frac{n\pi}{L}\right) \sin\left(\frac{n\pi x}{L}\right) q_n + \rho A \ddot{q}_n \sin\left(\frac{n\pi x}{L}\right) + k q_n \sin\left(\frac{n\pi x}{L}\right) + \beta \dot{q}_n \sin\left(\frac{n\pi x}{L}\right) = 0. \quad (2.10)$$

Dividing Eq.(2.10) with the $\sin\left(\frac{n\pi x}{L}\right)$ gives

$$\rho A \ddot{q}_n + \beta \dot{q}_n + \left[EI\left(\frac{n\pi}{L}\right)^4 - P(t)\left(\frac{n\pi}{L}\right)^2 + k \right] q_n = 0, \quad (2.11)$$

or

$$\ddot{q}_n + \frac{\beta}{\rho A} \dot{q}_n + \left[\frac{EI}{\rho A} \left(\frac{n\pi}{L}\right)^4 - \frac{P(t)}{\rho A} \left(\frac{n\pi}{L}\right)^2 + \frac{k}{\rho A} \right] q_n = 0. \quad (2.12)$$

In Eq.(2.12), the n^{th} fundamental frequency of a simply supported column when $P(t) = 0$ can be represented as $\omega_n = \left(\frac{n\pi}{L}\right)^2 \sqrt{\frac{EI}{\rho A}}$, whereas P_n is the n^{th} Euler buckling load and also known as Euler critical load. It is given as $P_n = EI\left(\frac{n\pi}{L}\right)^2$. Then Eq.(2.12) becomes

$$\ddot{q}_n + \frac{\beta}{\rho A} \dot{q}_n + \omega_n^2 \left[1 - \frac{P(t)}{P_n} + \frac{k}{P_n \left(\frac{n\pi}{L}\right)^2} \right] q_n = 0, \quad (2.13)$$

taking the stiffness co-efficient as α and the damping co-efficient as 2ζ in order to reduce the equation of motion, where

$$1 + \frac{k}{P_n \left(\frac{n\pi}{L}\right)^2} = \alpha, \quad (2.14)$$

$$\frac{\beta}{\rho A} = 2\zeta. \quad (2.15)$$

Eq.(2.12) can be transformed into

$$\ddot{q}_n + 2\zeta \dot{q}_n + \omega_n^2 \left[\alpha - \frac{P(t)}{P_n} \right] q_n = 0. \quad (2.16)$$

Eq.(2.16) has the damping term which cannot be solved by Pipes method of matrix solutions for finding the region of dynamic stability, so it requires further mathematical processing in order to reduce Eq.(2.16) to Hill equation.

2.3 Damping modification

Xie (2006) illustrated the method to eliminate the damping term and the first differentiation over time term, by simply using a change of variable. This intervention doesn't affect any of the solutions of the system. Applying the change in

the variable

$$q_n(t) = e^{-\zeta t} u_n(t), \quad (2.17)$$

the first and second derivative of Eq.(2.17) with respect to time can be given as

$$\dot{q}_n(t) = -\zeta e^{-\zeta t} u_n(t) + e^{-\zeta t} \dot{u}_n(t), \quad (2.18)$$

$$\ddot{q}_n(t) = \zeta^2 e^{-\zeta t} u_n(t) - 2\zeta e^{-\zeta t} \dot{u}_n(t) + e^{-\zeta t} \ddot{u}_n(t). \quad (2.19)$$

Substituting Eq.(2.18) and Eq.(2.19) into Eq.(2.16) yields

$$\begin{aligned} & \zeta^2 e^{-\zeta t} u_n(t) - 2\zeta e^{-\zeta t} \dot{u}_n(t) + e^{-\zeta t} \ddot{u}_n(t) - 2\zeta^2 e^{-\zeta t} u_n(t) \\ & + 2\zeta e^{-\zeta t} \dot{u}_n(t) + \omega_n^2 \left[\alpha - \frac{P(t)}{P_n} \right] e^{-\zeta t} u_n(t) = 0, \end{aligned} \quad (2.20)$$

Dividing Eq.(2.20) by $e^{-\zeta t}$ results in

$$\ddot{u}_n(t) + \omega_n^2 \left[-\frac{\zeta^2}{\omega_n^2} + \alpha - \frac{P(t)}{P_n} \right] u_n(t) = 0, \quad (2.21)$$

or

$$\ddot{u}_n(t) + \left(\omega_n^2 \alpha - \zeta^2 - \frac{P(t) \omega_n^2}{P_n} \right) u_n(t) = 0. \quad (2.22)$$

The fundamental frequency ω_n can be transformed to modified (damped) natural frequency ω_m , which can also be recognized as natural frequency of beam on elastic foundation. For simplification, a load factor μ (kN^{-1}) is assumed, which is inversely proportional to the critical buckling load of the beam. Therefore Eq.(2.22) can be transformed into

$$\ddot{u}_n(t) + \omega_m^2 [1 - \mu P(t)] u_n(t) = 0, \quad (2.23)$$

where

$$\omega_m^2 = \omega_n^2 \left[\alpha - \frac{\zeta^2}{\omega_n^2} \right], \quad (2.24)$$

$$\mu = \frac{\omega_n^2}{(\omega_n^2 \alpha - \zeta^2) P_n} = \frac{\omega_n^2}{\omega_m^2 P_n}. \quad (2.25)$$

In Eq.(2.23) the dynamic load $P(t)$ appears as a coefficient or parameter in the equation of motion, yielding a parametrically excited system. If $P(t)$ is a periodic function of period T , i.e. $P(t) = P(t + T)$, then Eq.(2.23) is a linear differential equation with periodic coefficient and is called a Hill equation. However, if $P(t)$ is a sinusoidal function of period T , Eq.(2.23) is called as Mathieu equation. Eq.(2.23) has no damping term and can be solved by using Pipes matrix method.

2.4 Summary

Different types of beam-foundation interactions and foundation behavior have been reviewed in this chapter. The equation of motion for beams on Winkler type foundation under dynamic axial loading has been derived. This equation is transformed into a Hill equation using damping modification. The Hill equation will be used for deriving the dynamic stability in the next chapter.

Chapter 3

Solution with Pipes Method

3.1 Introduction

A method for the solution of a class of linear, second-order differential equations with periodic coefficients of the Hill equation was presented by L. A. Pipes (2014). The method is adequate for the study of a large class of physical problems and is based on a procedure involving powers of matrices. This method not only provides the solution but also incorporates the stability behavior of the solution. Dynamic stability with various dynamic loadings is solved by the matrix method.

3.2 Solution for displacement

A considerable variety of physical problems leads to a formulation involving a differential equation that may be reduced to the general form of Eq.(3.1).

$$\frac{d^2u}{dt^2} + F(t)u = 0. \quad (3.1)$$

$F(t)$ is a periodic function of fundamental period T . A typical example is the case where the equation of motion of axially loaded beams on elastic foundations has reduced to Hill equation. Solution starts with the assumption that $x_1(t)$

and $x_2(t)$ be two linearly independent solutions of Eq.(3.1) in the fundamental interval $0 \leq t \leq T$. The value of $u(t)$ and its first derivative, $\dot{u}(t) = v(t)$, may be expressed in the following form for $0 \leq t \leq T$,

$$\begin{aligned} u(t) &= A_1 x_1(t) + A_2 x_2(t), \\ v(t) &= A_1 \dot{x}_1(t) + A_2 \dot{x}_2(t). \end{aligned} \tag{3.2}$$

or in the matrix form,

$$\begin{bmatrix} u(t) \\ v(t) \end{bmatrix} = \begin{bmatrix} u \\ v \end{bmatrix}_t = \begin{bmatrix} x_{11}(t) & x_{12}(t) \\ x_{21}(t) & x_{22}(t) \end{bmatrix} \cdot \begin{bmatrix} A_1 \\ A_2 \end{bmatrix}, \tag{3.3}$$

where A_1 and A_2 are arbitrary constants, and

$$\begin{bmatrix} x_{11}(t) & x_{12}(t) \\ x_{21}(t) & x_{22}(t) \end{bmatrix} = \begin{bmatrix} x_1(t) & x_2(t) \\ \dot{x}_1(t) & \dot{x}_2(t) \end{bmatrix}. \tag{3.4}$$

The determinant is found to be constant in the fundamental interval $0 \leq t \leq T$, and it can be written as

$$W_0 = \begin{vmatrix} x_{11}(t) & x_{12}(t) \\ x_{21}(t) & x_{22}(t) \end{vmatrix} = x_1(t)\dot{x}_2(t) - \dot{x}_1(t)x_2(t). \tag{3.5}$$

Since the two solutions $x_1(t)$ and $x_2(t)$ are linearly independent, $W_0 \neq 0$, and the matrix in Eq.(3.4) is non-singular and the inverse matrix can be generated. Furthermore, u and v for the initial condition can be obtained from Eq.(3.3) when $t = 0$,

$$\begin{bmatrix} u \\ v \end{bmatrix}_0 = \begin{bmatrix} x_{11}(0) & x_{12}(0) \\ x_{21}(0) & x_{22}(0) \end{bmatrix} \cdot \begin{bmatrix} A_1 \\ A_2 \end{bmatrix}, \tag{3.6}$$

or

$$\begin{bmatrix} A_1 \\ A_2 \end{bmatrix} = \frac{1}{W_0} \begin{bmatrix} x_{22}(0) & -x_{12}(0) \\ -x_{21}(0) & x_{11}(0) \end{bmatrix} \cdot \begin{bmatrix} u \\ v \end{bmatrix}_0. \quad (3.7)$$

This determines the column of arbitrary constants in terms of the given initial conditions. If Eq.(3.7) is substituted into Eq.(3.3), the result may be written in the form

$$\begin{bmatrix} u \\ v \end{bmatrix}_t = \frac{1}{W_0} \begin{bmatrix} x_{11}(t) & x_{12}(t) \\ x_{21}(t) & x_{22}(t) \end{bmatrix} \cdot \begin{bmatrix} x_{22}(0) & -x_{12}(0) \\ -x_{21}(0) & x_{11}(0) \end{bmatrix} \cdot \begin{bmatrix} u \\ v \end{bmatrix}_0. \quad (3.8)$$

The final values of u and v at the end of one interval of the variation of $F(t)$ are the initial values of u and v in the following interval. At the end of the fundamental period, when $t = T$, Eq.(3.8) becomes,

$$\begin{bmatrix} u \\ v \end{bmatrix}_T = \frac{1}{W_0} \begin{bmatrix} x_{11}(T) & x_{12}(T) \\ x_{21}(T) & x_{22}(T) \end{bmatrix} \cdot \begin{bmatrix} x_{22}(0) & -x_{12}(0) \\ -x_{21}(0) & x_{11}(0) \end{bmatrix} \cdot \begin{bmatrix} u \\ v \end{bmatrix}_0. \quad (3.9)$$

Taking equivalent matrix to Eq.(3.9)

$$\begin{bmatrix} u \\ v \end{bmatrix}_T = \begin{bmatrix} M \end{bmatrix} \begin{bmatrix} u \\ v \end{bmatrix}_0 = \begin{bmatrix} A & B \\ C & D \end{bmatrix} \cdot \begin{bmatrix} u \\ v \end{bmatrix}_0, \quad (3.10)$$

so that

$$\begin{bmatrix} M \end{bmatrix} = \begin{bmatrix} A & B \\ C & D \end{bmatrix} = \frac{1}{W_0} \begin{bmatrix} x_{11}(T) & x_{12}(T) \\ x_{21}(T) & x_{22}(T) \end{bmatrix} \cdot \begin{bmatrix} x_{22}(0) & -x_{12}(0) \\ -x_{21}(0) & x_{11}(0) \end{bmatrix}, \quad (3.11)$$

where A, B, C, D are the elements of the matrix resulting from multiplication of two matrices in Eq.(3.11),

$$\begin{aligned}
A &= \frac{1}{W_0} [x_{11}(T)x_{22}(0) - x_{12}(T)x_{21}(0)], \\
B &= \frac{1}{W_0} [x_{12}(T)x_{11}(0) - x_{11}(T)x_{12}(0)], \\
C &= \frac{1}{W_0} [x_{21}(T)x_{22}(0) - x_{22}(T)x_{21}(0)], \\
D &= \frac{1}{W_0} [x_{22}(T)x_{11}(0) - x_{21}(T)x_{12}(0)].
\end{aligned} \tag{3.12}$$

At the end of the second period of the variation of $F(t)$ we have

$$\begin{bmatrix} u \\ v \end{bmatrix}_{2T} = \begin{bmatrix} A & B \\ C & D \end{bmatrix} \begin{bmatrix} u \\ v \end{bmatrix}_T = \begin{bmatrix} A & B \\ C & D \end{bmatrix}^2 \begin{bmatrix} u \\ v \end{bmatrix}_0 = \begin{bmatrix} M \end{bmatrix}^2 \begin{bmatrix} u \\ v \end{bmatrix}_0. \tag{3.13}$$

The solution after the end of n periods can be written as

$$\begin{bmatrix} u \\ v \end{bmatrix}_{nT} = \begin{bmatrix} A & B \\ C & D \end{bmatrix}^n \begin{bmatrix} u \\ v \end{bmatrix}_0 = \begin{bmatrix} M \end{bmatrix}^n \begin{bmatrix} u \\ v \end{bmatrix}_0. \tag{3.14}$$

Eq.(3.14) is the solution of Hill equation at any time $t > 0$ in terms of the initial conditions and two linearly independent solutions of Hill equation in the fundamental interval $0 \leq t \leq T$.

3.3 Stability of solution

If the lateral vibration of a beam under periodic axial load $P(t)$ with any given end conditions is to be stable, it is necessary and sufficient that the functions $u(t)$ remains bounded for all values of the time t . At the end of n complete cycles of the oscillation of the periodical loading, $t = nT$.

Conditions for dynamic stability are based on latent root of $[M]^n$, following to that, Pipes presented a condition from Eq.(3.14),

$$\left| A + D \right| < 2, \quad \textit{Stable Vibration.} \quad (3.15)$$

In Eq.(3.15), elements of $[M]^n$ become trigonometric function and the $u(t)$ remains bounded. In such a case, the beam performs stable vibration under the action of periodic axial loading.

On the other hand, if the value of $|A + D|$ exceeds the value 2, then the elements of $[M]^n$ becomes the hyperbolic function which increases exponentially with the number of cycles n performed by the periodic loading. In such a case, the beam performs the unstable vibrations,

$$\left| A + D \right| \geq 2, \quad \textit{Unstable Vibration.} \quad (3.16)$$

Moreover, the boundary separating stable and unstable vibration is that $|A + D|$ is equals to 2. Concisely, to determine the stability of beam under the assumed conditions, it is only necessary to compute the value of $|A + D|$.

The general theory will now be applied to the solution of some representative, special cases. Thus, if $P(t)$ is in the form of any periodical loading such as rectangular(step), exponential, sawtooth, or sinusoidal it can be solved by Pipes method.

3.4 Rectangular loading

The Hill equation in Eq.(2.23) is solved for the particular case where the function $P(t)$ has the form of rectangular ripple. Let T be the fundamental period of the rectangular ripple, and let the ripple vary in the height of $+H$ to $-H$ as

shown in Fig. 3.1. The Hill equation may be represented in a piecewise manner, throughout the first cycle of its variation. If the first mode of vibration ($n = 1$) is considered, subscript n can be omitted from Eq.(2.23) for ease in calculation.

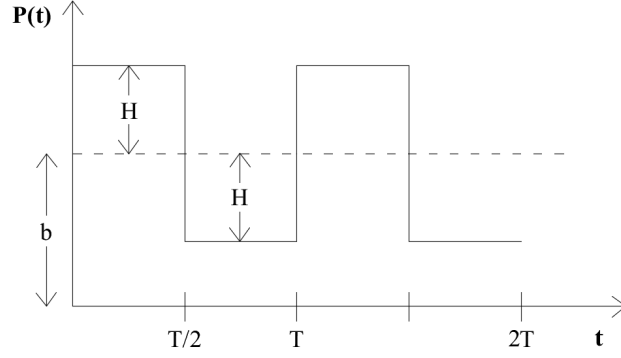


Figure 3.1: Rectangular/Step axial loading

Loading pattern is given as,

$$P(t) = b + H \quad \text{for } 0 < t \leq \frac{T}{2}, \quad (3.17)$$

$$P(t) = b - H \quad \text{for } \frac{T}{2} < t \leq T. \quad (3.18)$$

Now, Eq.(2.23) can be written as,

$$\ddot{u}(t) + \omega_m^2 [1 - \mu(b + H)]u(t) = 0 \quad \text{for } 0 < t \leq \frac{T}{2}, \quad (3.19)$$

$$\ddot{u}(t) + \omega_m^2 [1 - \mu(b - H)]u(t) = 0 \quad \text{for } \frac{T}{2} < t \leq T. \quad (3.20)$$

Introducing,

$$g_1 = \omega_m \sqrt{1 - \mu(b + H)}, \quad (3.21)$$

$$g_2 = \omega_m \sqrt{1 - \mu(b - H)}, \quad (3.22)$$

therefore Eq.(3.21) and Eq.(3.22) may be written in following form,

$$\ddot{u}(t) + g_1^2 u(t) = 0 \quad \text{for } 0 < t \leq \frac{T}{2}, \quad (3.23)$$

$$\ddot{u}(t) + g_2^2 u(t) = 0 \quad \text{for } \frac{T}{2} < t \leq T. \quad (3.24)$$

The first solution for Eq.(3.23) can written in matrix form for interval $0 < t \leq \frac{T}{2}$, using *Cosine* function as the solution

$$\begin{bmatrix} u \\ v \end{bmatrix}_t = \begin{bmatrix} \cos(g_1 t) & \frac{1}{g_1} \sin(g_1 t) \\ -g_1 \sin(g_1 t) & \cos(g_1 t) \end{bmatrix} \begin{bmatrix} u_0 \\ v_0 \end{bmatrix}. \quad (3.25)$$

The subscripts at the bottom of the column matrices in Eq.(3.25) refer to the time at which u and v must be evaluated. Here, u_0 and v_0 are the initial value for time $t = 0$, and u_t and v_t are the value at any time t as the subscript is t . Now taking $t = \frac{T}{2}$, where $c_1 = g_1 \cdot \frac{T}{2}$, we have

$$\begin{bmatrix} u \\ v \end{bmatrix}_{\frac{T}{2}} = \begin{bmatrix} \cos(c_1) & \frac{1}{g_1} \sin(c_1) \\ -g_1 \sin(c_1) & \cos(c_1) \end{bmatrix} \begin{bmatrix} u_0 \\ v_0 \end{bmatrix}. \quad (3.26)$$

Now taking interval $\frac{T}{2} < t \leq T$, where $c_2 = g_2 \cdot \frac{T}{2}$, we have

$$\begin{bmatrix} u \\ v \end{bmatrix}_T = \begin{bmatrix} \cos(c_2) & \frac{1}{g_2} \sin(c_2) \\ -g_2 \sin(c_2) & \cos(c_2) \end{bmatrix} \begin{bmatrix} u \\ v \end{bmatrix}_{\frac{T}{2}}. \quad (3.27)$$

Since the values of u and v at $t = \frac{T}{2}$ are the initial value of next interval, $\frac{T}{2} < t \leq T$, we have

$$\begin{bmatrix} u \\ v \end{bmatrix}_T = \begin{bmatrix} \cos(c_1) & \frac{1}{g_1} \sin(c_1) \\ -g_1 \sin(c_1) & \cos(c_1) \end{bmatrix} \begin{bmatrix} \cos(c_2) & \frac{1}{g_2} \sin(c_2) \\ -g_2 \sin(c_2) & \cos(c_2) \end{bmatrix} \begin{bmatrix} u_0 \\ v_0 \end{bmatrix}. \quad (3.28)$$

If we perform multiplication in Eq.(3.28) and re-writing it in form of $[M]$ as shown in equation below,

$$\begin{bmatrix} u \\ v \end{bmatrix}_T = \begin{bmatrix} A & B \\ C & D \end{bmatrix} \begin{bmatrix} u_0 \\ v_0 \end{bmatrix} = [M] \begin{bmatrix} u_0 \\ v_0 \end{bmatrix}. \quad (3.29)$$

Here, $[M]$ can be written as

$$[M] = \begin{bmatrix} \cos c_1 \cos c_2 - \frac{g_1}{g_2} \sin c_1 \sin c_2 & \frac{1}{g_1} \sin c_1 \cos c_2 - \cos c_1 \sin c_2 \\ -g_2 \sin c_1 \cos c_2 - g_1 \sin c_1 \cos c_2 & -\frac{g_2}{g_1} \sin c_1 \sin c_2 + \cos c_1 \cos c_2 \end{bmatrix}. \quad (3.30)$$

The boundary condition for the stability can be given as $|\frac{A+D}{2}| = 1$,

$$\left| \frac{A+D}{2} \right| = \cos c_1 \cos c_2 - \frac{1}{2} \left[\frac{g_1}{g_2} + \frac{g_2}{g_1} \right] \sin c_1 \sin c_2, \quad (3.31)$$

or

$$\left| \frac{A+D}{2} \right| = \cos c_1 \cos c_2 - \frac{1}{2} \left[\frac{c_1^2 + c_2^2}{c_1 c_2} \right] \sin c_1 \sin c_2, \quad (3.32)$$

where $\frac{g_1}{g_2} + \frac{g_2}{g_1} = \frac{\frac{T^2}{4}[g_1^2 + g_2^2]}{\frac{T^2}{4}g_1 g_2} = \frac{c_1^2 + c_2^2}{c_1 c_2}$.

Substituting the value of c_1 , c_2 , and respectively substituting the value of g_1 and g_2 from Eq.(3.21) and Eq.(3.22) into the boundary condition given in Eq.(3.32)

yields

$$\begin{aligned} \frac{A+D}{2} &= \cos \left[\omega_m \frac{T}{2} \sqrt{1 - \mu(b+H)} \right] \cos \left[\omega_m \frac{T}{2} \sqrt{1 - \mu(b-H)} \right] \\ &\quad - \frac{1}{2} \sin \left[\omega_m \frac{T}{2} \sqrt{1 - \mu(b+H)} \right] \sin \left[\omega_m \frac{T}{2} \sqrt{1 - \mu(b-H)} \right] \\ &\quad \left[\frac{2(1 - \mu b)}{\sqrt{(1 - \mu b)^2 - (\mu H)^2}} \right]. \end{aligned} \quad (3.33)$$

Introducing ratio of frequencies as $\gamma = \frac{2\pi}{2\omega_m}$, which is ratio of the exciting frequency to twice the natural frequency, so that the condition for dynamic stability is given as

$$\begin{aligned} \frac{A+D}{2} &= r = \cos \left[\frac{\pi}{2\gamma} \sqrt{1 - \mu(b+H)} \right] \cos \left[\frac{\pi}{2\gamma} \sqrt{1 - \mu(b-H)} \right] \\ &\quad - \frac{1}{2} \sin \left[\frac{\pi}{2\gamma} \sqrt{1 - \mu(b+H)} \right] \sin \left[\frac{\pi}{2\gamma} \sqrt{1 - \mu(b-H)} \right] \\ &\quad \left[\frac{2(1 - \mu b)}{\sqrt{(1 - \mu b)^2 - (\mu H)^2}} \right]. \end{aligned} \quad (3.34)$$

The value of r from Eq.(3.34) decides whether the system is stable or unstable using conditions listed below,

- $|r| \geq 1$ for Unstable,
- $|r| < 1$ for stable.

3.5 Sawtooth type loading

The dynamic stability of the Hill equation in Eq.(2.23) is solved for the sawtooth type dynamic axial loading as shown in Fig. 3.2. The function $P(t)$ is given in a form as shown below, this function is for interval $0 \leq t \leq T$ and repeats the variation after each cycle of T . The minimum amplitude of loading is b , whereas

the maximum amplitude of loading can be $h = aT + b$. Loading $P(t)$ can be defined as

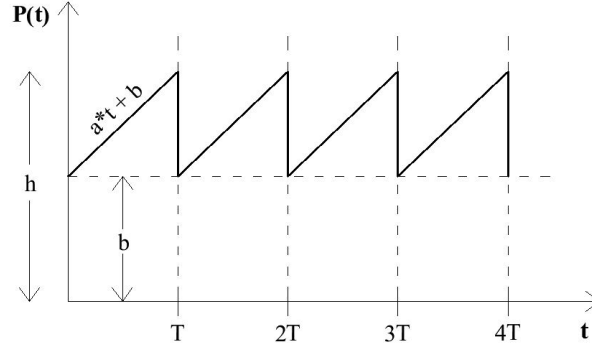


Figure 3.2: Sawtooth axial loading

$$P(t) = at + b \quad 0 \leq t \leq T. \quad (3.35)$$

Therefore, Hill equation takes form of

$$\ddot{u}(t) + \omega_m^2 [1 - \mu(at + b)]u(t) = 0. \quad (3.36)$$

Introducing

$$z = \omega_m^2 [1 - \mu(at + b)] \quad (3.37)$$

and the change of variable from t to the z transforms Eq.(3.36) into

$$\frac{d^2 u}{dz^2} + \frac{z}{\mu^2 a^2 \omega_m^4} u = 0. \quad (3.38)$$

Solution of Eq.(3.38) is based on Bessel functions of order one third multiplied with constant. The solution for u can be given as

$$u = z^{\frac{1}{2}} [A_1 J_{\frac{1}{3}}(kz^{\frac{3}{2}}) + A_2 Y_{\frac{1}{3}}(kz^{\frac{3}{2}})], \quad (3.39)$$

where A_1 and A_2 are arbitrary constants, and

$$k = \frac{2}{-3a\mu\omega_m^2}. \quad (3.40)$$

According to Eq.(3.39), two linearly independent roots can be obtained as

$$x_1(t) = z^{\frac{1}{2}}J_{\frac{1}{3}}(kz^{\frac{3}{2}}), \quad x_2(t) = z^{\frac{1}{2}}Y_{\frac{1}{3}}(kz^{\frac{3}{2}}), \quad (3.41)$$

the following derivatives can be calculated (Pipes and Harvill, 2014):

$$\frac{dx_1}{dt} = zJ_{-\frac{2}{3}}(kz^{\frac{3}{2}}), \quad \frac{dx_2}{dt} = zY_{-\frac{2}{3}}(kz^{\frac{3}{2}}). \quad (3.42)$$

Therefore, the solution of Eq.(3.36) in the fundamental interval $0 \leq t \leq T$ may be expressed in the following form:

$$\begin{bmatrix} u \\ v \end{bmatrix}_t = \begin{bmatrix} z^{\frac{1}{2}}J_{\frac{1}{3}}(kz^{\frac{3}{2}}) & z^{\frac{1}{2}}Y_{\frac{1}{3}}(kz^{\frac{3}{2}}) \\ zJ_{-\frac{2}{3}}(kz^{\frac{3}{2}}) & zY_{-\frac{2}{3}}(kz^{\frac{3}{2}}) \end{bmatrix} \begin{bmatrix} u \\ v \end{bmatrix}_0. \quad (3.43)$$

Introducing following notations of $kz^{\frac{3}{2}}$ for time $t = 0$ and $t = T$, such as

$$\theta = kb^{\frac{3}{2}} = -\frac{2b^{\frac{3}{2}}}{3a\mu\omega_m^2}, \quad \text{for } t = 0, \quad (3.44)$$

$$\phi = kh^{\frac{3}{2}} = -\frac{2h^{\frac{3}{2}}}{3a\mu\omega_m^2}, \quad \text{for } t = T. \quad (3.45)$$

The determinant is given by

$$W_0 = \begin{vmatrix} b^{\frac{1}{2}}J_{\frac{1}{3}}(\theta) & b^{\frac{1}{2}}Y_{\frac{1}{3}}(\theta) \\ bJ_{-\frac{2}{3}}(\theta) & bY_{-\frac{2}{3}}(\theta) \end{vmatrix} = b^{\frac{3}{2}}[J_{\frac{1}{3}}(\theta)Y_{-\frac{2}{3}}(\theta) - J_{-\frac{2}{3}}(\theta)Y_{\frac{1}{3}}(\theta)]. \quad (3.46)$$

The matrix of $[M]$ of Eq.(3.11) for interval $0 \leq t \leq T$ can be obtained as,

$$\begin{bmatrix} M \end{bmatrix} = \begin{bmatrix} A & B \\ C & D \end{bmatrix} = \frac{1}{W_0} \begin{bmatrix} h^{\frac{1}{2}} J_{\frac{1}{3}}(\phi) & h^{\frac{1}{2}} Y_{\frac{1}{3}}(\phi) \\ h J_{-\frac{2}{3}}(\phi) & h Y_{-\frac{2}{3}}(\phi) \end{bmatrix} \begin{bmatrix} b Y_{-\frac{2}{3}}(\theta) & -(b)^{\frac{1}{2}} Y_{\frac{1}{3}}(\theta) \\ -b J_{-\frac{2}{3}}(\theta) & b^{\frac{1}{2}} J_{\frac{1}{3}}(\theta) \end{bmatrix}. \quad (3.47)$$

Therefore, the value of A and D can be taken as,

$$A = \frac{b(h)^{\frac{1}{2}}}{W_0} [J_{\frac{1}{3}}(\phi) Y_{-\frac{2}{3}}(\theta) - J_{-\frac{2}{3}}(\theta) Y_{\frac{1}{3}}(\phi)], \quad (3.48)$$

$$D = \frac{h(b)^{\frac{1}{2}}}{W_0} [J_{\frac{1}{3}}(\theta) Y_{-\frac{2}{3}}(\phi) - J_{-\frac{2}{3}}(\phi) Y_{\frac{1}{3}}(\theta)]. \quad (3.49)$$

Hence similar to last section, dynamic stability conditions can be applied using Eq.(3.48) and Eq.(3.49),

- $|\frac{A+D}{2}| \geq 1$ for unstable vibrations,
- $|\frac{A+D}{2}| < 1$ for stable vibrations.

Bessel functions can be represented by dominant term of their asymptotic expansions (Pipes and Harvill, 2014) such as

$$\begin{aligned} J_{\frac{1}{3}}(e) &= \left(\frac{2}{\pi e}\right)^{\frac{1}{2}} \cos(e - \pi/4 - \pi/6), \\ Y_{\frac{1}{3}}(e) &= \left(\frac{2}{\pi e}\right)^{\frac{1}{2}} \sin(e - \pi/4 - \pi/6), \\ J_{-\frac{2}{3}}(e) &= \left(\frac{2}{\pi e}\right)^{\frac{1}{2}} \cos(e - \pi/4 - \pi/3), \\ Y_{-\frac{2}{3}}(e) &= \left(\frac{2}{\pi e}\right)^{\frac{1}{2}} \sin(e - \pi/4 - \pi/3). \end{aligned} \quad (3.50)$$

Using dominant terms the determinant W_0 from Eq.(3.46) and the matrix $[M]$

from Eq.(3.47) can be given as

$$W_0 = \frac{-3a\mu\omega_m^2}{\pi}, \quad (3.51)$$

and matrix $[M]$ can be written as

$$\left[M \right] = \frac{-2}{3a\mu\omega_m^2} \left(\frac{bh}{\phi\theta} \right)^{\frac{1}{2}} \cdot \begin{bmatrix} b^{\frac{1}{2}} \cos(\theta - \phi) & \sin(\phi - \theta) \\ (bh)^{\frac{1}{2}} \sin(\theta - \phi) & h^{\frac{1}{2}} \cos(\theta - \phi) \end{bmatrix}. \quad (3.52)$$

Therefore boundary condition for dynamic stability can be rewritten in diminished form,

$$\frac{A + D}{2} = \frac{\cos(\theta - \phi)}{3a\mu\omega_m^2} [bh^{\frac{1}{2}} + hb^{\frac{1}{2}}]. \quad (3.53)$$

The same stability criteria can be applied as explained in previous sections. It should be noted that the ratio of frequencies (γ) term cannot be introduced in this solution as sawtooth loading is a function of time as shown in Eq.(3.35). However, dynamic stability for any given condition of such loading can be assessed.

3.6 Sum of step functions

When $P(t)$ of Hill equations is a sum of step functions as shown in Fig. 3.3 can be effectively solved by the matrix method.

Assuming that function $P(t)$ is made up of δ number of step functions, each has length T_0 and heights $H_1, H_2, H_3, \dots, H_\delta$, so that

$$\delta T_0 = T. \quad (3.54)$$

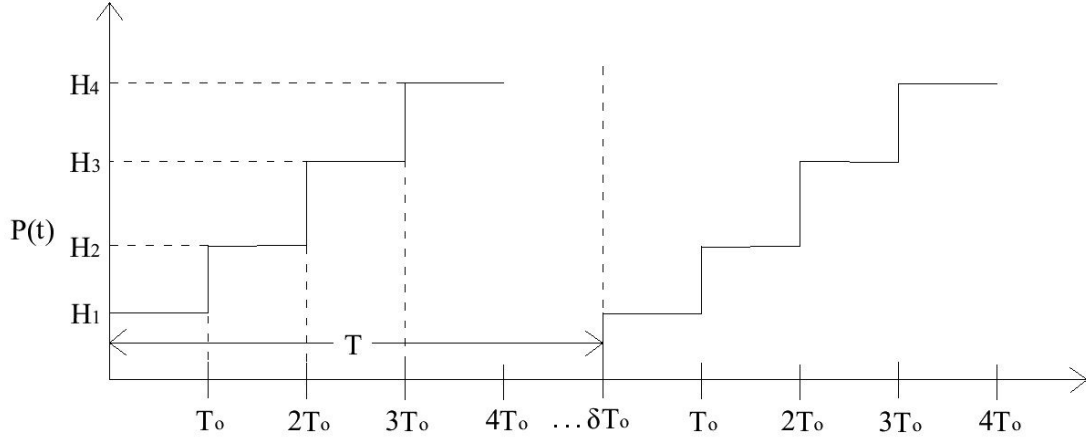


Figure 3.3: Sum of step functions

For ease of calculations, introducing the following notations as

$$g_k = \sqrt{H_k}, \quad \phi_k = T_0 \sqrt{H_k}, \quad (3.55)$$

where k is any real number as $0 \leq k \leq \delta$, from which matrix $[M]_k$ can be generated as

$$[M]_k = \begin{bmatrix} P_k & Q_k \\ R_k & P_k \end{bmatrix} = \begin{bmatrix} \cos(\phi_k) & \frac{1}{g_k} \sin(\phi_k) \\ -g_k \sin(\phi_k) & \cos(\phi_k) \end{bmatrix}. \quad (3.56)$$

In such a case, multiplication of matrices can be written as

$$\begin{bmatrix} A & B \\ C & D \end{bmatrix} = [M]_\delta \cdot [M]_{\delta-1} \cdots [M]_2 \cdot [M]_1 = [M]. \quad (3.57)$$

Now solution for u can be carried out using Eq.(3.57) for first period T

$$\begin{bmatrix} u \\ v \end{bmatrix}_T = \begin{bmatrix} A & B \\ C & D \end{bmatrix} \begin{bmatrix} u_0 \\ v_0 \end{bmatrix}. \quad (3.58)$$

Similarly, the solution after any n periods, when $t = nT$, can be presented as,

$$\begin{bmatrix} u \\ v \end{bmatrix}_{nT} = \begin{bmatrix} A & B \\ C & D \end{bmatrix}^n \begin{bmatrix} u_0 \\ v_0 \end{bmatrix}. \quad (3.59)$$

Now, the dynamic stability criteria shown in Eq.(3.15) and Eq.(3.16) can simply applied and the dynamic stability can be assessed.

3.7 Exponential variation of loadings

Following the solution strategy used in the previous section 3.6, Pipes method can be used to study the dynamic stability and obtain the approximate solution of Hill equation by representing the given loading function in $P(t)$ throughout the fundamental interval by sum of step functions.

Loading is taken in generalized form of exponential loading of period T , which will be divided in δ number of identical T_0 intervals, in order to generate δ numbers of individual step loadings such as $H_1, H_2, H_3, \dots H_\delta$. The generalized form of exponential loading can be defined as

$$P(t) = y^2 e^{-2t} - v^2, \quad 0 \leq t \leq T, \quad (3.60)$$

where, y and v are any nonzero numbers, hence Hill equation can be written as

$$\ddot{u}(t) + \omega_m^2 [1 - \mu(y^2 e^{-2t} - v^2)] u(t) = 0. \quad (3.61)$$

Eq.(3.61) can be solved with Bessel functions and sum of step loadings, solution with Bessel functions will be the same as that given in section 3.5. This solution can solve Hill equation for the whole fundamental interval T . However, solution with the sum of step functions method shown in section 3.6 is an approximate

solution and accuracy of this approximation solution depends upon the number of δ . Higher number of δ tends to provide more accurate approximation, however that results in extended calculations.

Almost any given function $P(t)$ can be represented with step function by dividing the fundamental interval T into any δ subintervals of length $T_0 = \frac{T}{\delta}$. Hence in the k th interval, the height of the representative step function can be determined by

$$H_k = \frac{1}{T_0} \int_{(k-1)T_0}^{kT_0} P(t)dt, \quad k = 1, 2, 3, \dots \delta. \quad (3.62)$$

Using H_k , $[M]_k$ can be generated as shown in Eq.(3.56) and accordingly $[M]$ can be calculated as Eq.(3.57).

Now the dynamic stability criteria shown in Eq.(3.15) and Eq.(3.16) can be simply applied and the dynamic stability can be assessed.

3.8 Summary

The general solutions of the Hill equation of beams on elastic foundations have been presented using Pipes matrix method, which also encompasses the assessment of the stability nature of the solution. Various excitations such as rectangular (step), sawtooth, a sum of step, and exponential are theoretically solved for the dynamic stability.

Chapter 4

Numerical Analysis

In order to demonstrate the method discussed in Chapter 3, numerical results are obtained, which incorporate solving the Hill equation in various cases for the response of the system and also assessing the dynamic stability of systems. The dynamic stability diagrams are also generated.

4.1 Dynamic stability diagram under periodic rectangular loading

To find the dynamic stability diagram under periodic rectangular loading, it is vital to set the parameter and assume the properties of a specimen. For the numerical calculations, a steel strip with reasonably assumed geometric property is considered, which has a length of 457.2 mm, width of 31.75 mm, and thickness of 3.18 mm. Steel has a density of 7850 kg/m³, and an elastic modulus of 2.10×10^5 N/mm². Natural frequency and Euler critical load when $n = 1$ can be calculated as

$$\omega_n = \left(\frac{n\pi}{L}\right)^2 \sqrt{\frac{EI}{\rho A}} = 223.75 \text{ rad/s} = 35.63 \text{ Hz},$$

$$P_n = EI\left(\frac{n\pi}{L}\right)^2 = 840 \text{ N}.$$

Reasonable assumptions are made from the references (Engel, 1991; Saha et al.,

1997) for the value of stiffness of foundation k , which is taken as 20 kN/m² and the damping ratio 2ζ is combined damping of foundation and beam, which is taken as 2 %.

So, $\alpha = 1.505$ and $\omega_m = 274.5$ rad/s = 43.71 Hz can be calculated from Eq.(2.14) and Eq.(2.24). Moreover $\mu = 0.000791$ can be obtained from Eq.(2.25).

As practical beams will have some amount of static load all the time, so $b = 100$ N is taken. The value of H will be varying from 0 - 840 N, and the aim is to assess the dynamically buckling before the actual static buckling. Moreover, the value of the ratio of frequencies(γ) which is the ratio of excitation frequency to twice the natural frequency of beam-foundation system is taken in a range of 0 - 1.25. As the unknown parameters in dynamic stability condition shown in Eq.(3.34) are the dynamic force ($b + H$) and ratio of frequencies(γ). The values of both parameters are placed in equations. From the different values of dynamic loads($b + H$) and ratio of frequencies(γ), only those values are kept separate which give $|r| \geq 1$ in Eq.(3.34), these values of dynamic loads ($b + H$) and ratio of frequencies(γ) give unbounded solution of Hill equation and result in dynamically unstable vibrations. Plotting these values of ($b + H$) vs. γ result in dynamic stability diagram of the beam on elastic foundation under the action of periodic rectangular loading.

Fig. 4.1 shows the dynamic stability diagram under periodic rectangular loading. The solid line represents the dynamic stability boundary which separates the dynamically stable and unstable regions. The area enclosed in this solid line represents dynamically unstable regions whereas the rest of the area in the plot tends to be dynamically stable. The dynamic instability region shown close to $\gamma = 1$ is the principal region of dynamic instability. However, dynamic instability regions close to $\gamma = 0.48, 0.24$ are also obtained which are shown in Fig. 4.2 and

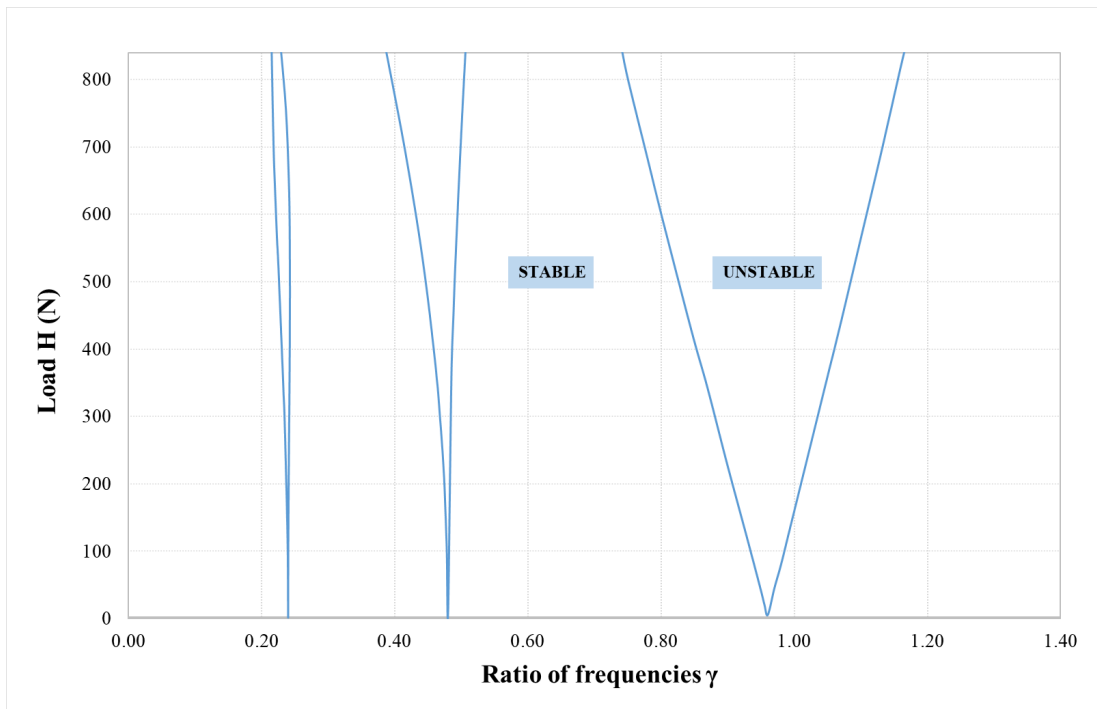


Figure 4.1: Dynamic stability diagram for periodic rectangular loading

Fig. 4.3, respectively.

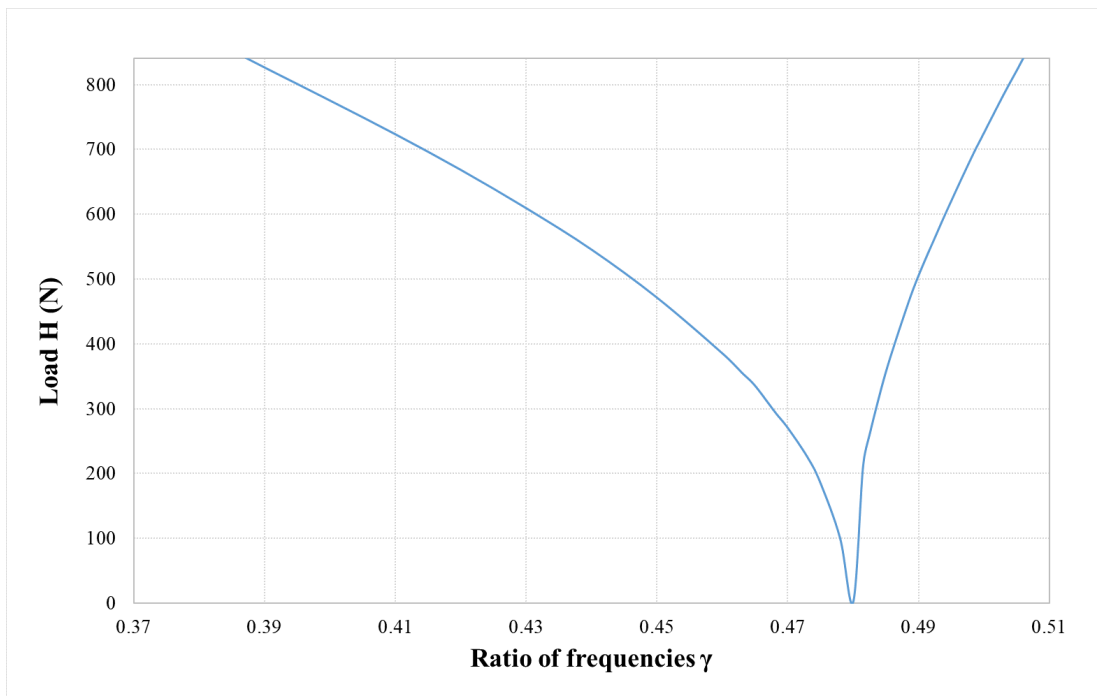


Figure 4.2: Dynamic stability diagram for periodic rectangular loading, $\gamma = 0.48$

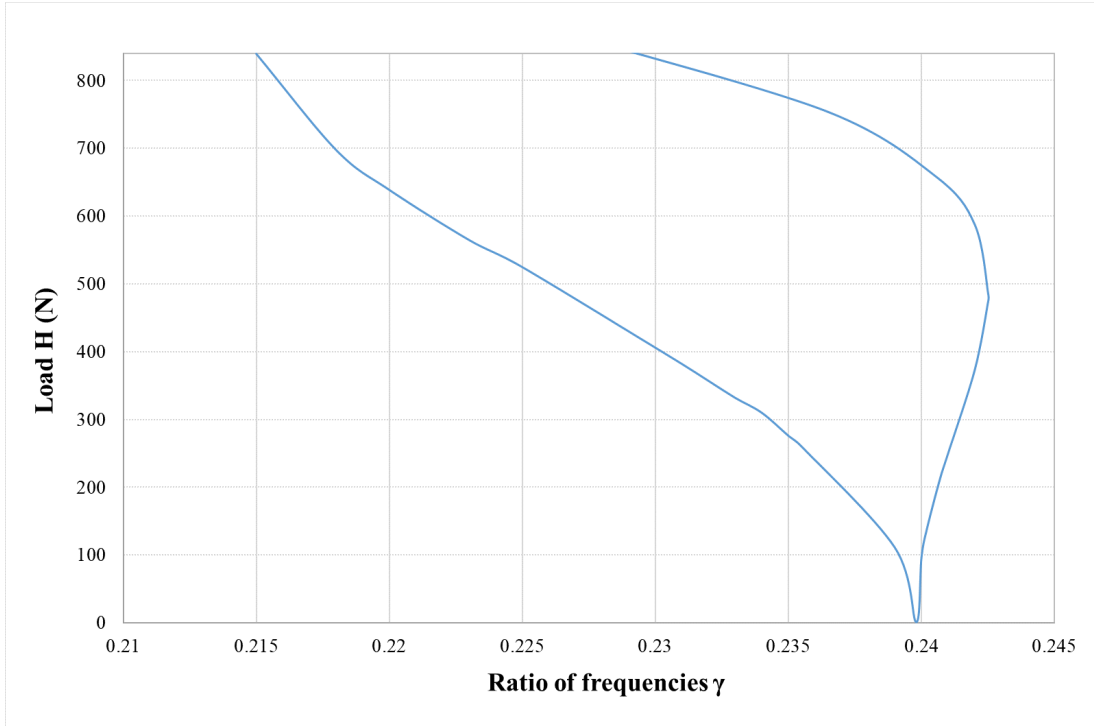


Figure 4.3: Dynamic stability diagram for periodic rectangular loading, $\gamma = 0.24$

According to the dynamic stability diagram shown in Fig. 4.1, all three unstable regions start from nearly zero dynamic loading, meaning even really small such as 10 N force can generate the dynamic unstable vibration if it has excitation frequency twice the natural frequency ω_m of the beam on elastic foundations. Realistically, it might not be possible to get unstable vibration with nearly zero amplitude, the causes of such inaccuracy are the damping of beam and soil, the friction between surfaces and joints, etc.

4.1.1 Parametric study

For a broader understanding of behavior of the solutions, it is vital to conduct a parametric study. Starting with the change in stiffness of foundation k , where $k = 1 \text{ kN/m}^2$, $k = 20 \text{ kN/m}^2$ and $k = 40 \text{ kN/m}^2$ are taken separately and the principle dynamic instability regions are compared.

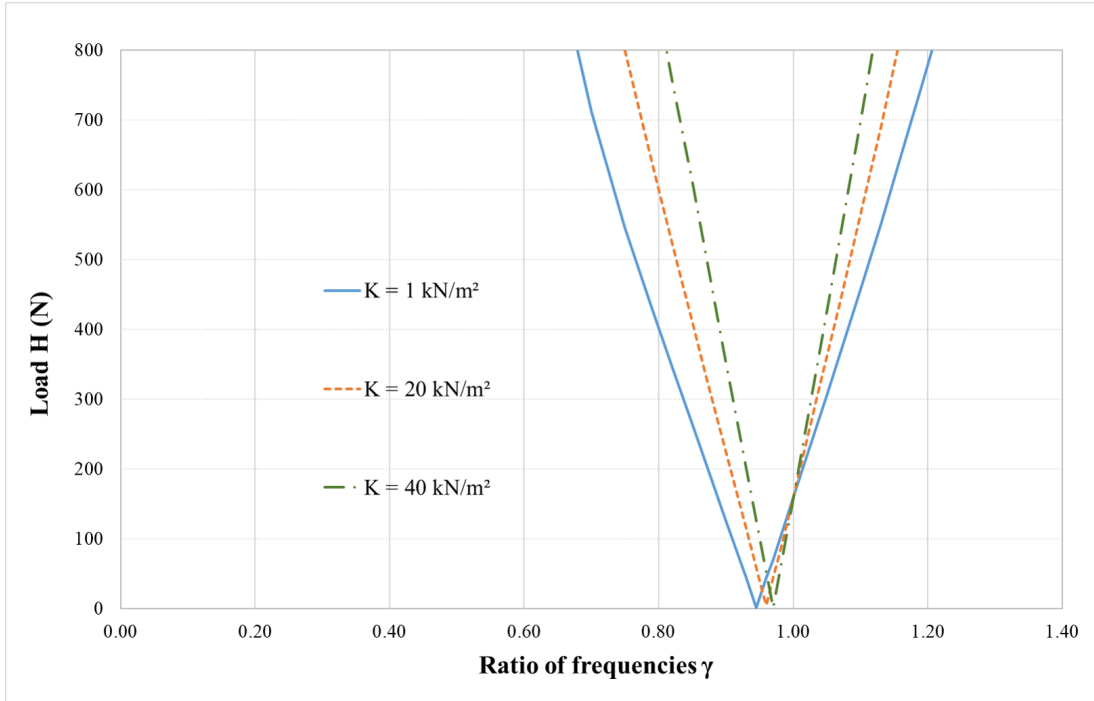


Figure 4.4: Dynamic stability diagrams for $k = 1, 20, 40 \text{ kN/m}^2$

Fig. 4.4 shows that the origins of all three principal dynamic stability regions remain nearly the same, whereas the width of these regions is changed. Moreover, an increase in width of dynamic stability region is observed as a result of a decrease in the stiffness of foundation. This result is evident as the rigidity of lateral support increase, and it permits less vibration of the beam. In other words, the area of dynamic stability region for $k = 1 \text{ kN/m}^2$ is the maximum, and for $k = 40 \text{ kN/m}^2$ is the minimum. Therefore it can be said that area(width) of the principal region of dynamic stability is inversely proportional to the stiffness of a foundation for any identical cases of geometry and loading profile.

The loading is considered static and dynamic in nature. Thus, it becomes essential to study the impact of the change in static loading on the dynamic stability region. Here, the static load b is changed such that $b = 0 \text{ N}$, $b = 100 \text{ N}$, $b = 200 \text{ N}$, and the remaining parameters of the system are kept constant. The principal regions of dynamic stability diagrams are plotted in Fig. 4.5.

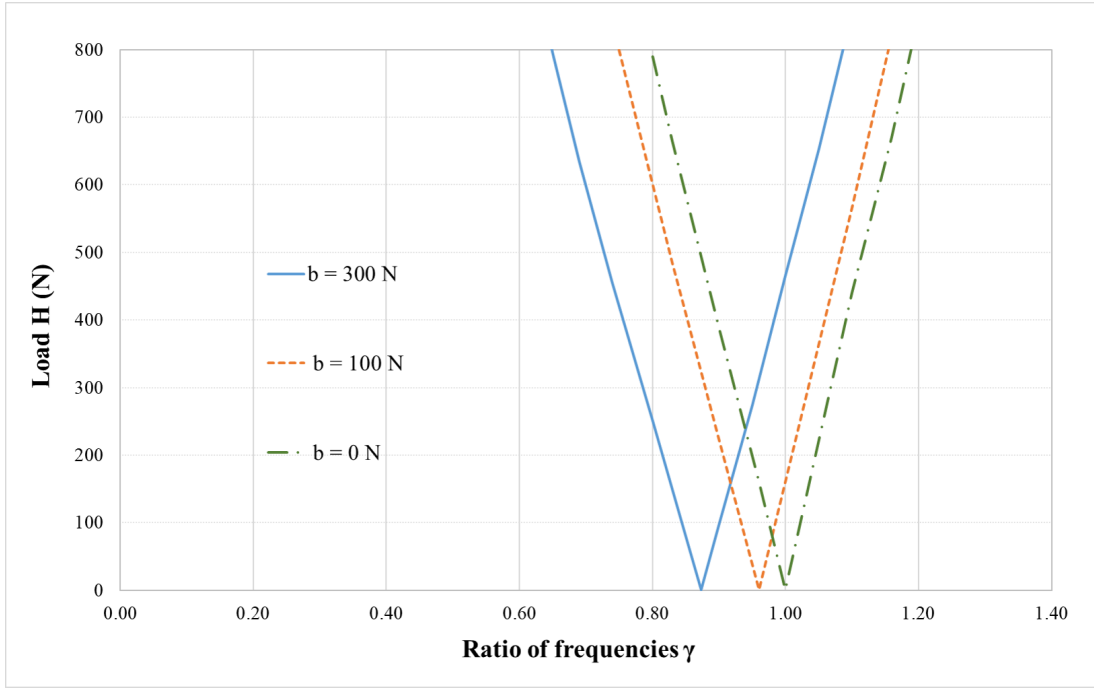


Figure 4.5: Dynamic stability diagrams for $b = 0, 100, 200$ N

Fig. 4.5 shows that the area of all three dynamic stability regions remains the same with the change in static load. However, the origin point tends to move towards left by virtue of an increase in static loading. Moreover, pure dynamic loading when $b = 0$, gives the dynamic stability diagram originating at $\gamma = 1$, where the excitation frequency is twice the modified natural frequency of the beam. Hence, slightly away from the origin of principal dynamic instability region for $\gamma = 1$ with $b = 100$ N in Fig. 4.1 is justified with discussion above.

Dynamic stability diagrams in Fig. 4.1 are based on first mode of vibration, where $n = 1$. Change in n will change the fundamental frequency(ω_n), Euler critical load(P_n), stiffness co-efficient(α) given in Eq.(2.14) and consequently it will also change the natural frequency(ω_m). Considering the first three modes of vibration, the principal dynamic stability regions are developed by taking $n = 1$, $n = 2$, and $n = 3$, where, $b = 0$ and $H = 0 - 840$ N. Fig. 4.6 presents the first three regions of instability, corresponding to the first three modes of vibration of the beam on elastic foundations.

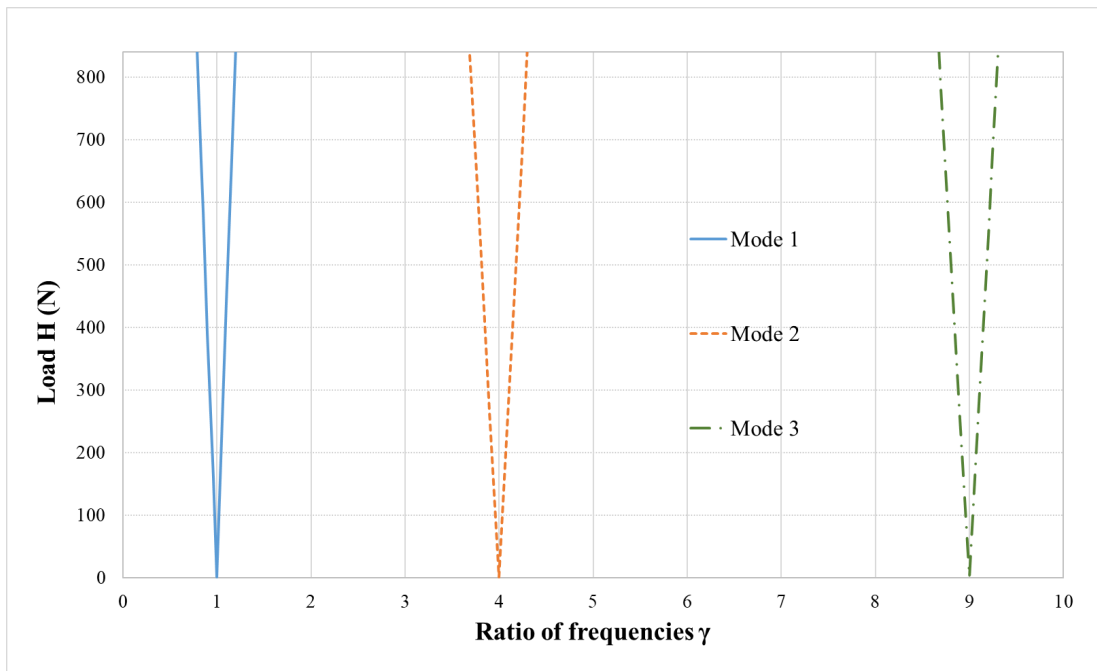


Figure 4.6: Dynamic stability diagrams for $n = 1, 2, 3$

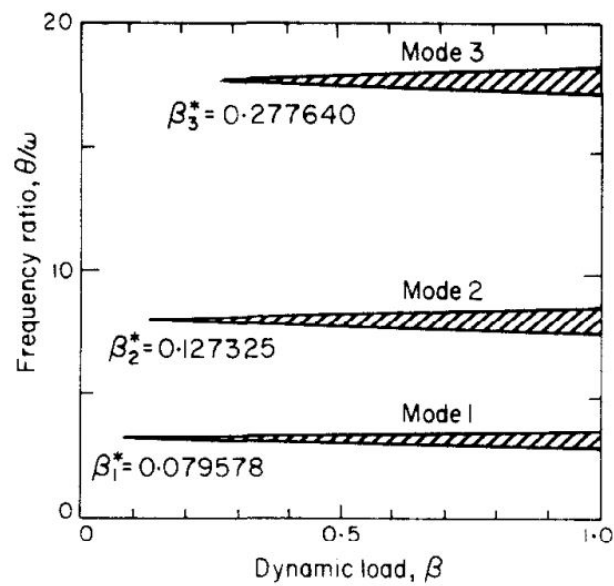


Figure 4.7: Results of beam on elastic foundation with "Floquet theory" (Engel, 1991)

Fig. 4.7 shows dynamic instability regions, which were developed to study the effect of damping. The noticeable part of this result is as we move further on axis of the ratio of frequencies, the width of dynamic instability regions increases. In

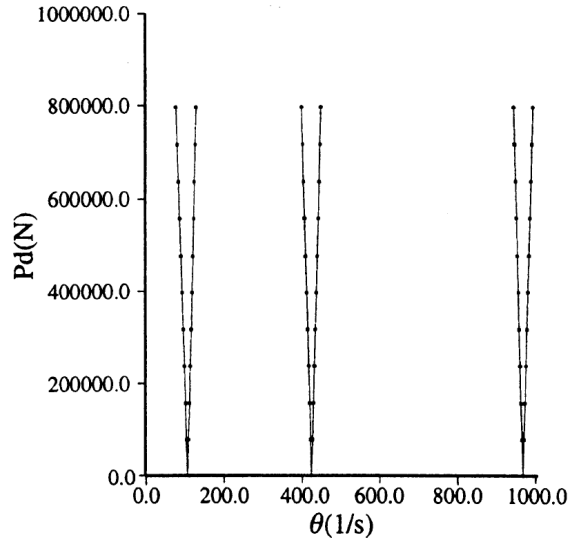


Figure 4.8: Results HEB 200 beam using finite element method (Briseghella et al., 1998)

other words, as the vibration mode transforms from $n = 1$ to $n = 2$, and $n = 2$ to $n = 3$, the width and overall area of dynamic instability regions increases. Similar results are obtained with Pipes matrix method in Fig. 4.6, the width of the region of dynamic unstable regions increases with an increase in mode shape. Unlike in the study presented in Fig. 4.8, when finite element method was used, dynamic instability regions have identical width and area for all modes.

As the mode transforms from $n = 1$ to $n = 2$, the fundamental frequency(ω_n) changes, and other parameters such as ω_m , α , and μ also change. It can be easily anticipated that the dynamic stability diagram generated from $n = 2$ cannot be as same as the dynamic stability diagram generated from $n = 1$. Therefore, it can be said that the modal analysis with the Pipes method (Fig. 4.6) and Floquet theory (Fig. 4.7) have produced more reasonable results.

4.2 Dynamic stability assessment - Sum of step loadings

The exponential load $P(t)$ shown in Eq.(3.60) is used for the system to assess the dynamic stability, where certain parameters are set to be fixed and the approximation solution using the method described in section 3.6 is used. The constants of loading $P(t)$ are assumed as shown in Eq.(4.1), where the period is assumed to be $T = 0.5$ s for the excitation loading. Assuming $\delta = 10$ may give $T_0 = 0.05$ s. The excitation is

$$P(t) = 36\pi^2 e^{-2t} - \frac{1}{25}, \quad \text{where } 0 \leq t \leq 0.5. \quad (4.1)$$

Therefore, $\delta = 10$ will generate $H_1, H_2, H_3, \dots, H_{10}$ values, which can be calculated using Eq.(3.62). The parameters g_k and ϕ_k can be calculated as

$$g_k = \omega_m \sqrt{1 - \mu(H_k)}, \quad (4.2)$$

$$\phi_k = T_0 * \omega_m \sqrt{1 - \mu(H_k)}, \quad (4.3)$$

where k is any real number between $0 \leq k \leq \delta$, furthermore $P_k = \cos(\phi_k)$, $Q_k = \frac{1}{g_k} \sin(\phi_k)$, $R_k = -g_n \sin(\phi_k)$ can be calculated accordingly.

Using the data in Table 4.1, the matrix $[M]$ can be calculated for every k value, for example, if $k = 1$, then $[M]_1$ can be expressed as,

$$[M]_1 = \begin{bmatrix} P_1 & Q_1 \\ R_1 & P_1 \end{bmatrix} = \begin{bmatrix} 0.6499 & -0.0032 \\ -177.963 & 0.6499 \end{bmatrix}. \quad (4.4)$$

The final matrix $[M]$ is obtained by multiplication of the chain of matrices in

Table 4.1: Values of matrix components

Step	H_k	g_k	ϕ_k	P_k	Q_k	R_k
1	338.078	234.145	11.707	0.6499	-0.0032	177.963
2	305.902	238.171	11.909	0.7887	-0.0026	146.437
3	276.788	241.756	12.088	0.8856	-0.0019	112.282
4	250.444	244.954	12.248	0.9482	-0.0013	77.784
5	226.607	247.813	12.391	0.9838	-0.0007	44.430
6	205.039	250.371	12.519	0.9986	-0.0002	13.111
7	185.523	252.664	12.633	0.9981	0.0002	-15.705
8	167.864	254.720	12.736	0.9864	0.0006	-41.837
9	151.886	256.567	12.828	0.9671	0.0010	-65.288
10	137.429	258.227	12.911	0.9427	0.0013	-86.176

the form, $[M] = [M]_{10} \cdot [M]_9 \cdot [M]_8 \cdot \dots \cdot [M]_1$, which can be written as

$$[M] = \begin{bmatrix} A & B \\ C & D \end{bmatrix} = \begin{bmatrix} -0.15615 & -0.00406 \\ 239.06215 & -0.17772 \end{bmatrix}. \quad (4.5)$$

As a result, boundary condition for this case can be expressed as

$$\left| A + D \right| = 0.3338 < 2, \quad \text{Stable Vibration.} \quad (4.6)$$

It can be said that, for the given loading type, the system will generate dynamically stable vibration.

4.3 Comparison of solutions

In order to evaluate the reliability of the solution using Pipes matrix method, it is essential to make a comparison with the solutions obtained by other methods such as finite element method and Floquet theory for dynamic stability.

Considering the HEB 200 beam with geometric property given as length $L = 7m$, moment of inertia $I = 2.003 \times 10^{-8} \text{ m}^4$, and mass per unit length $m = \rho A = 61.3$

kg/m, modulus of elasticity $E = 2.1 \times 10^{11}$ N/m². The beam is simply supported and axially loaded. In this case, foundation is not considered, which means the $k = 0$ N/m². Loading has the form $P(t) = P_d \cos(\theta t)$, where P_d is the amplitude, θ is the excitation frequency, and t represents time. Hill equation of this case can be written as

$$\ddot{u}(t) + \omega_m^2 [1 - \mu(P_d \cos(\theta t))]u(t) = 0. \quad (4.7)$$

Eq.(4.7) has the form of Mathieu equation, for which the first fundamental frequency and Euler critical load can be calculated as

$$\omega_n = \left(\frac{n\pi}{L}\right)^2 \sqrt{\frac{EI}{\rho A}} = 52.762 \text{ rad/s},$$

$$P_n = EI\left(\frac{n\pi}{L}\right)^2 = 847235 \text{ N}.$$

Solution to such problem is provided with Pipes matrix method. The loading is taken as the sum of δ number of step functions, $\delta = 10$ is considered so that $T_0 = T/10$, and $H_1, H_2, H_3, \dots, H_{10}$ can be obtained from Eq.(3.62).

Manual solution to this problem in order to develop a dynamic instability diagram can be done by following the steps as follows.

- **Step - 1** Assume any value of excitation frequency (θ) and find the period of excitation T and T_0 . It should be noted that the assumption of excitation frequency should be $1.5 \leq \frac{\theta}{\omega_n} \leq 2.5$ in order to generate first principal region of dynamic instability. As parametric resonance occurs when excitation frequency is double or in folds with a natural frequency.
- **Step - 2** The step loading H_k can be determined using Eq.(3.62) where $P(t) = P_d \cos\left(\frac{2\pi}{T}t\right)$. Assume any value of P_d less than Euler buckling load ($P_d < P_n$), because any axial force larger than Euler critical force will buckle the beam.

- **Step - 3** The value of $g_k = \sqrt{H_k}$ and $\phi_k = T_0\sqrt{H_k}$ can be calculated based on the value of H_k .
- **Step - 4** Using the g_k and ϕ_k , values of P_k , Q_k , R_k and related matrix $[M]_k$ can be calculated using Eq.(3.56). Multiplication of these matrices can be obtained as $[M]$ shown in Eq.(3.57).
- **Step - 5** Following the value of $[M]$, $|A + D|/2$ can be obtained which determines the dynamic stability condition of the given point. In order to plot the dynamic instability boundaries, the value of $|A + D|/2$ is required to be 1.

Therefore, if the value of $|A + D|/2 < 1$ for assumed value of P_d , one should increase the assumed value of P_d and repeat the whole calculation from Step - 2. Moreover, if the $|A + D|/2 > 1$, one should decrease the assumed value of P_d . It is required to keep on changing the assumed value of P_d and repeating the calculation till $|A + D|/2 = 1$ is achieved. However, if for all values of P_d , $|A + D|/2 < 1$ is obtained, one should change the assumed value of excitation frequency (θ) and follow the procedure starting from Step 1.

For a further illustration taking an example of any Point- D on dynamic stability diagram which has an excitation frequency $\theta = 95$ rad/s, period $T = 0.0661$ s, and ratio of frequencies $\gamma = \frac{2\pi/T}{2\omega_n} = 0.90$. Assumed value of $P_d = 336500$ N is taken. Further, values of H_k , g_k , ϕ_k , P_k , Q_k , and R_k are calculated which are shown in Table 4.2.

Therefore, multiplication of matrices $[M]$ can be presented as,

$$\begin{bmatrix} M \end{bmatrix} = \begin{bmatrix} A & B \\ C & D \end{bmatrix} = \begin{bmatrix} -1.000468561 & -0.013061175 \\ -0.022517515 & -0.999825626 \end{bmatrix}. \quad (4.8)$$

Table 4.2: Value of matrix component for $\theta = 95$ rad/s, $P_d = 336500$ N

Step	H_k	g_k	ϕ_k	P_k	Q_k	R_k
1	315512.8	41.80	0.276	0.9622	3.05E-06	-303580.8
2	194948.9	46.30	0.306	0.9537	4.892E-06	-185918.5
3	225.0	52.75	0.348	0.9400	0.004177	-211.5
4	-194585.0	58.51	0.386	0.9264	-4.76E-06	180257.3
5	-315373.4	61.80	0.408	0.9180	-2.91E-06	289497.5
6	-315445.1	61.81	0.408	0.9179	-2.91E-06	289561.7
7	-195519.0	58.53	0.386	0.9263	-4.74E-06	181109.8
8	-753.3	52.79	0.348	0.9399	-0.001248	708.1
9	194298.9	46.32	0.306	0.9536	4.908E-06	-185289.7
10	314978.6	41.82	0.276	0.9621	3.055E-06	-303054.9

As a result, $|A + D|/2 = 1.00014 \approx 1$, so it can be said that Point- D lies on the dynamic stability boundary.

Following to the calculation procedure described above, more points lying on the dynamic stability boundary can be obtained which are given in Table 4.3.

Table 4.3: Reference points for dynamic stability boundary

Points	$\theta(\text{rad/s})$	$P_d(\text{N})$	$ A + D /2$
A	79.14	882500	1.00010
B	84.42	693000	1.00055
C	94.97	650000	1.15667
D	94.97	336500	1.00014
E	105.52	1	1
F	126.63	280000	0.75322
G	116.08	365000	1.00063
H	126.63	755000	1.00041
I	130.32	902100	0.99996

Accuracy in the value of $|A+D|/2$ is maintained up to three decimal places. Point- C is in the unstable region, whereas Point- F is in the stable region. Dynamic stability diagram for the axially loaded HEB 200 beam can be plotted with respect to excitation frequency(θ) as shown in Fig. 4.9. Similarly the dynamic stability diagram can be plotted with respect to ratio of frequencies ($\gamma = \frac{2\pi/T}{2\omega_n} = \frac{\theta}{2\omega_n}$) as

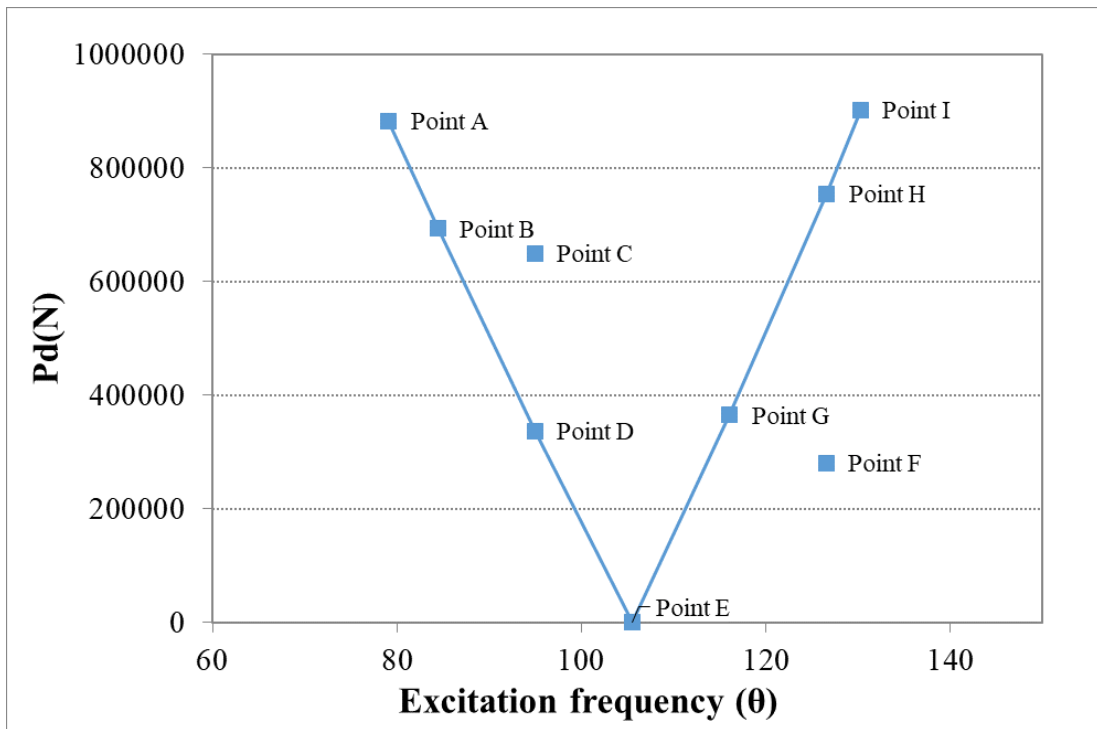


Figure 4.9: Dynamic stability diagrams for HEB 200 beam

shown in Fig. 4.10.

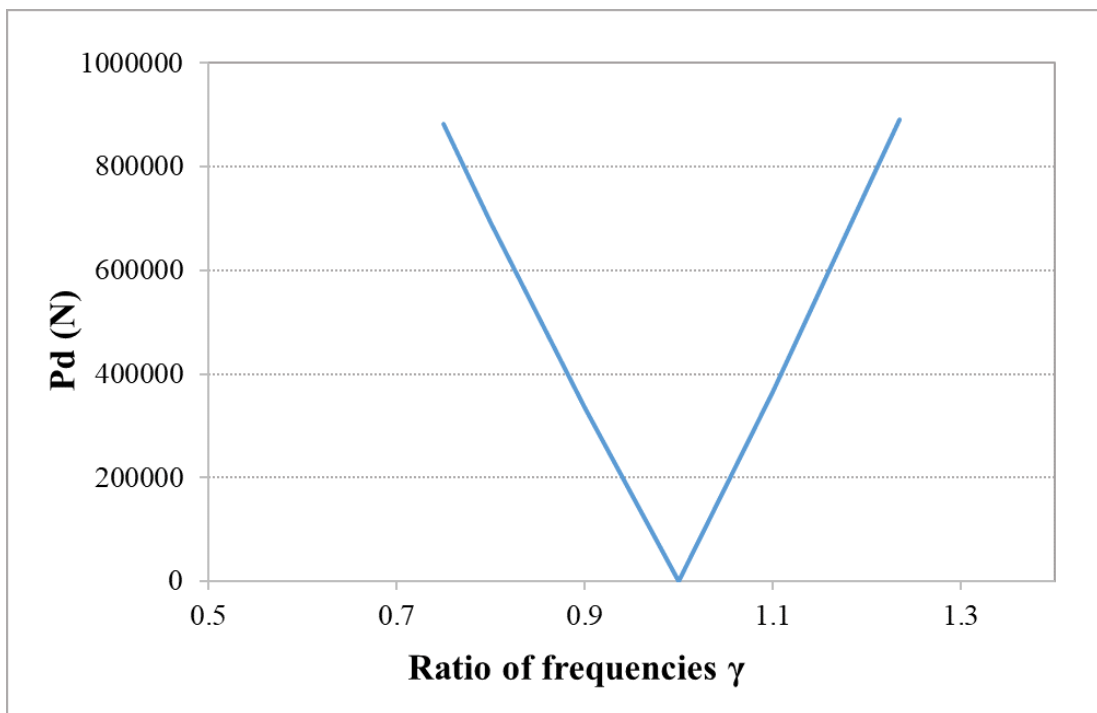


Figure 4.10: Dynamic stability diagram with respect to ratio of frequencies (γ)

In order to make a comparison, dynamic stability diagram obtained with Pipes method is overlapped with dynamic stability results obtained with Floquet method (theoretical method) and finite element method (Briseghella et al., 1998).

From Fig. 4.11 it can be noted that Pipes solution is slightly shifted from both the theoretical solution as well as finite element solution, except that it is nearly coincidental. Hence, it can be said that the dynamic stability results computed using Pipes matrix method are identical with results obtained using traditional methods.

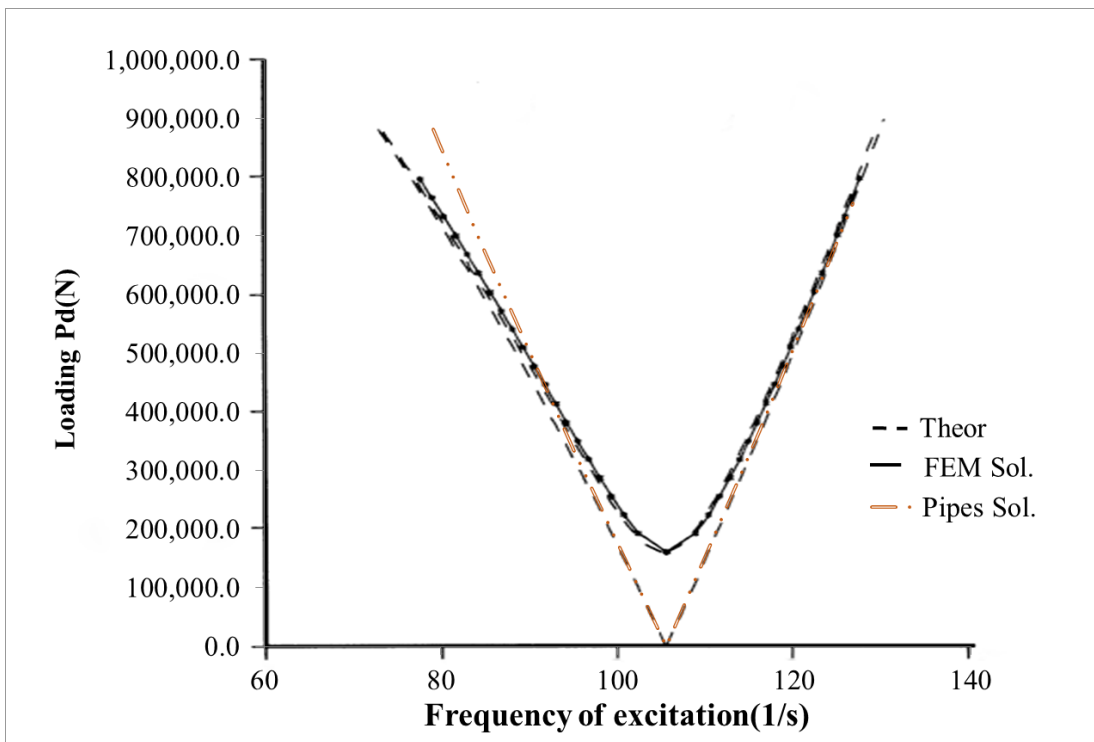


Figure 4.11: Comparison of solutions with Floquet theory, finite element method and Pipes Method

4.4 Summary

Dynamic stability diagrams have been plotted using Pipes method for several excitation cases. A parametric study shows that the dynamic instability regions

shrink while an increase in stiffness of supporting foundation. The dynamic instability region shifts towards origin if the static loading is increased. Modal study results of dynamic stability of beam on elastic foundations reveal that the area of dynamic instability regions increases with higher mode vibrations. Successful comparison of results is also obtained.

Chapter 5

Dynamic Stability of Rock Slopes

5.1 Introduction

Civil engineering works such as tunnel construction, open pit mining, road construction, and foundation pit excavation inevitably involve several rock slope problems. Accurate evaluation of rock slope stability and its influencing factors not only provides a scientific basis for engineering construction but also plays an essential role in guiding slope reinforcement and landslide prediction. Therefore, the stability of rock slope is of vital importance against blasting vibrations and machinery vibrations. The blasting vibrations will laterally excite a rock slope, and propagation of such vibrations are fast through the rock slab. The dynamic stability of rock slab becomes essential to assess for mining cases where blasting is widely used. The blasting vibrations can be measured with the sampling data collection, which are in arbitrary forms. Therefore, the dynamic stability of rock slope resting on rock layer can be assessed with the Pipes method.

5.2 Geology of the rock slope

Geology of a specific case can be described as a rock resting on a rock layer base. The top end is loose, and the rock bottom is considered as a pin joint. A case study based on similar geology was conducted on Highwood pass, Alberta (Hu and Cruden, 1993). However, Hu and Cruden only considered the static buckling of the rock slope. After knowing the nature of loading, one can assess the buckling of the rocks due to dynamic instability under blasting vibrations. The geological profile for two sites of Highwood pass is given here in Table 5.1.

Table 5.1: Geological profile (Hu and Cruden, 1993)

	Site 1	Site 2
Bedding thickness (m)	0.7	0.05
Inertia moment (m ⁴)	$2.858 * 10^{-2}$	$1.042 * 10^{-5}$
Estimated uniaxial compressive strength (MPa)	300	200
Estimated lower and upper bounds of the	3-300	2-200
Young's modulus (GPa)		
Unit weight (kN/m ³)	25	25

These sites are composed of rock layers of limestone, quartzite, chert, dolostone, shale, and sandstone.

5.3 Stress waves from blasting

Blasting vibrations are believed to be one of the most harmful factors of all hazards arising from blasting. The blasting seismic wave produces disturbance in the rock mass, which spreads in the form of a stress wave. In the near and middle-field of blasting source where the stress wave peak is higher than the tensile strength of the rock, the blasting destroys the rock, resulting in crushed zones, fracture zones or blasting damage. In the far-field of blasting source where the stress

wave peak is lower than the tensile strength of the rock, the blasting causes elastic stress waves that vibrate rock particles which may cause the potential damage in the rock and earth mass to develop further, thus leading to slope instability, landslides, and other damages. The strong vibration caused by blasting load is very likely to trigger landslides, avalanches, etc. Therefore, the study of blasting vibration impact on rock slope stability is of major practical significance.

For the purpose of engineering assessments and design, the dynamic load generated from an explosion in the ground can be anticipated from the Peak Particle Velocity (PVV). The PVV from a coupled explosion can be given in the following general form (Zhou and Zhao, 2011):

$$V = J \left[\frac{Z}{Q^B} \right]^{-n}, \quad (5.1)$$

where J and n are constants relating on geological profile and explosion setup, Z is the actual distance (m), Q is the charge weight (kg). The exponent B is a function of the geometry of the explosives charge and reflects the energy transmission from the explosive to the surrounding medium. Many mining applications tend to use 1/2, or square root scaling, while most military and civil engineering applications tend to use 1/3, or cubic root scaling.

The parameters J and n are generally a function of the soil/rock quality but can be affected by the other factors such as types of explosives and scale of the explosion.

The peak particle velocity can be excited as a harmonic function (sinusoidal wave) using the velocity-displacement relationship :

$$V = 2\pi f z, \quad (5.2)$$

where V is the velocity, f is the frequency (Hz), and z is the displacement of particles. Therefore, excitation can be taken as a harmonic function, and dynamic stability of rock under such excitation can be assessed.

5.4 Methodology

In order to derive an equation of motion for a simply supported rock slope resting on an elastic rock layer under axial loading, an infinitesimal element of the system with Δx length is taken with the free body diagram as shown in Fig. 5.1. Where, P is the applied axial loading, S is shear loading and M is for the bending moment. Taking ρ as density, A as cross-sectional area such that D'Alembert's force is $\rho A \Delta x \ddot{v} = m \ddot{v}$, where v is the transverse displacement of the beam. The forces exerted from the foundation remains the same as $kv \Delta x$ and $\beta \dot{v} \Delta x$.

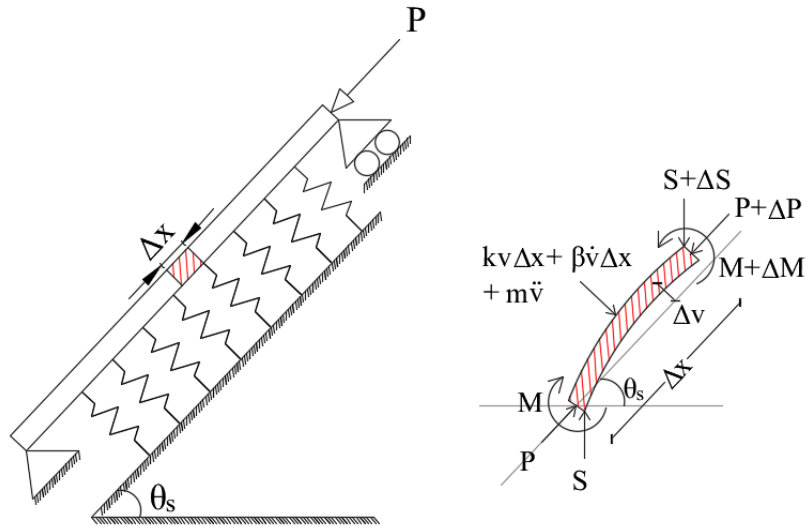


Figure 5.1: Rock slope under axial loading and free body diagram

Summing up all vertical forces results in

$$\Delta S + (\rho A \Delta x \ddot{v} + kv \Delta x + \beta \dot{v} \Delta x) \cos(\theta_s) + \Delta P \sin(\theta_s) = 0. \quad (5.3)$$

Now summing up the horizontal forces gives

$$(\rho A \Delta x \ddot{v} + kv \Delta x + \beta \dot{v} \Delta x) \sin(\theta_s) - \Delta P \cos(\theta_s) = 0. \quad (5.4)$$

Eq.(5.4) can be rewritten in terms of ΔP , therefore

$$\Delta P = (\rho A \Delta x \ddot{v} + kv \Delta x + \beta \dot{v} \Delta x) \tan(\theta_s). \quad (5.5)$$

Substituting Eq.(5.3) into Eq.(5.5) yields

$$\Delta S + (\rho A \Delta x \ddot{v} + kv \Delta x + \beta \dot{v} \Delta x) \cos(\theta_s) + (\rho A \Delta x \ddot{v} + kv \Delta x + \beta \dot{v} \Delta x) \sin(\theta_s) \tan(\theta_s) = 0, \quad (5.6)$$

or

$$\Delta S + (\rho A \Delta x \ddot{v} + kv \Delta x + \beta \dot{v} \Delta x)(\cos(\theta_s) + \sin(\theta_s) \tan(\theta_s)) = 0. \quad (5.7)$$

When $\Delta x \rightarrow 0$, Eq.(5.7) can be written as

$$\frac{\partial S}{\partial x} = -(\rho A \ddot{v} + kv + \beta \dot{v}) \sec(\theta_s). \quad (5.8)$$

Summing up the moments at midpoint results in

$$-P \Delta v + S \Delta x \cos(\theta_s) - \Delta M = 0, \quad (5.9)$$

or

$$\frac{\partial M}{\partial x} = S \cos(\theta_s) - P(t) \frac{\partial v}{\partial x}. \quad (5.10)$$

As P is a function of time t , it can be written as $P(t)$. Moreover, differentiating

Eq.(5.10) with respect to x yields,

$$\frac{\partial^2 M}{\partial x^2} = \frac{\partial S}{\partial x} \cos(\theta_s) - P(t) \frac{\partial^2 v}{\partial x^2}. \quad (5.11)$$

Now using Euler-Bernoulli relationship $M = EI(\frac{\partial^2 v}{\partial x^2})$ and eliminating S from Eq.(5.11) using Eq.(5.8) results in

$$EI(\frac{\partial^4 v}{\partial x^4}) = -(\rho A(\frac{\partial^2 v}{\partial t^2}) + kv + \beta(\frac{\partial v}{\partial t})) \cos(\theta_s) \sec(\theta_s) - P(t)(\frac{\partial^2 v}{\partial x^2}), \quad (5.12)$$

or

$$EI(\frac{\partial^4 v}{\partial x^4}) + P(t)(\frac{\partial^2 v}{\partial x^2}) + \rho A(\frac{\partial^2 v}{\partial t^2}) + kv + \beta(\frac{\partial v}{\partial t}) = 0. \quad (5.13)$$

Eq.(5.13) represents the equation of motion for the axially loaded rock slope resting on elastic rock layer or soil, which is the same as Eq.(2.7). Hence, it can be said that Pipes solution can be applied to any configuration of beams and elastic foundations without any alteration. However, change in the boundary condition of beam-column can affect the equation of motion as well as the dynamic stability solution for the beams on elastic foundations.

5.5 Results and discussion

In order to assess the dynamic stability and buckling of the rock slope, Highwood pass case is chosen as an example because future constructions will require the blasting around the sites which may cause dynamic buckling of the rocks in the region (Hu and Cruden, 1993). Geological property is taken from Table 5.1. The rock has the length (l) = 20 m, depth (h) = 0.7 m, width (b) = 1 m, density (ρ) = 2548 kg/m³ and the Young's modulus (E) = 150 GPa. From the given data the fundamental frequency $\omega_n = (\frac{n\pi}{L})^2 \sqrt{\frac{EI}{\rho A}} = 38.25$ rad/s = 6.09 Hz and the Euler buckling force, $P_n = EI(\frac{n\pi}{L})^2 = 105794$ kN, can be obtained for the rock beam.

Stiffness of the elastic foundation $k = 20$ MPa is taken, which results in $\alpha = 8.67$ from Eq.(2.14), therefore the natural frequency of the beam on elastic foundations can be calculated as $\omega_m = 17.93$ Hz from Eq.(2.24). Moreover $\mu = 1.09 \times 10^{-9}$ can be obtained from Eq.(2.25). Dynamic stability diagram of the rock on elastic foundations can be derived for the harmonic cosine function as shown in Fig. 5.2.

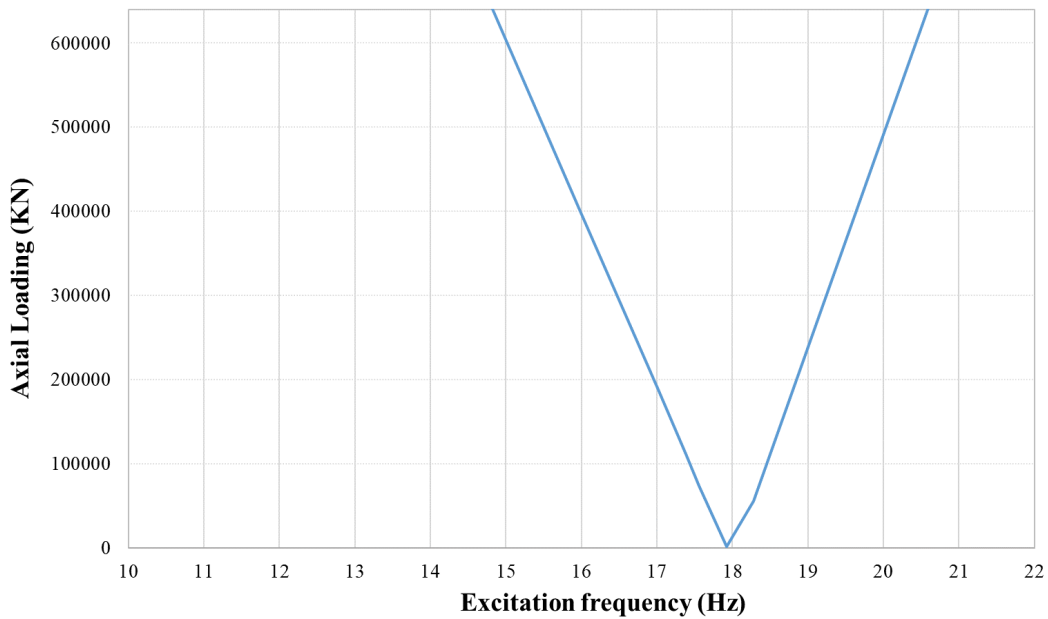


Figure 5.2: Dynamic buckling diagram of rock slope on elastic foundations

Dynamic buckling of the rock slope can be assessed up to the excitation loading $\frac{1}{\mu} = \alpha P_n = 9.17 \times 10^5$ kN from Eq.(2.23). The elastic foundation acts as a support so that the system can bear more amplitude of axial loading in the form of blasting than the Euler critical load. However, the modified natural frequency of the rock slope and elastic foundation (ω_m) is higher than the natural frequency of the rock beam (ω_n) itself due to the effect of the foundation. A increase in the natural frequency mainly depends upon the stiffness of the foundation. Alazzawi (2017) presented similar results about the natural frequency of beams on elastic foundations.

Blasting pressure can be calculated using the formula provided by Newmark and Hansen (1961), which can be written as

$$P_s = 6784 \frac{W}{R^3} + 93 \sqrt{\frac{W}{R^3}} \text{ (bar)}, \quad (5.14)$$

where P_s is the shock pressure in bar, W is the charge mass expressed in kilograms of TNT and R is distance from the centre of a spherical charge in meter.

Mills (1987) suggested the following for blasting incidental pressure,

$$P_s = \frac{1772}{z^3} + \frac{114}{z^2} + \frac{108}{z} - 0.019 \text{ kPa}, \quad (5.15)$$

where z is scale distance,

$$z = \frac{R}{W^{\frac{1}{3}}}. \quad (5.16)$$

If 1 T of TNT equivalent charge is used at 35 m away from rock slope, the incidental pressure $P_s = 81723 \text{ N/m}^2$ using Eq.(5.14), whereas $P_s = 88943 \text{ N/m}^2$ can be obtained with Eq.(5.15). Both pressure equations yield almost identical anticipation of incidental blasting pressure. Furthermore, the total incidental loading H can be obtained by multiplying the cross-sectional area of the rock slope to the incidental pressure, $H = 37.9 \text{ MN}$.

Fig. 5.3 shows that the blasting load with the frequency ranges from 17.75 Hz to 18.2 Hz can buckle the rock slope even with very small load compared to the buckling load of the rock beam. As the blast scaling distance decreases, the range of frequency causing the dynamic buckling increases, which is illustrated in Fig. 5.4, where R is the distance between the center of charge and the rock slope. The rock slope tends to be more dynamically stable with an increase in distance from blasting.

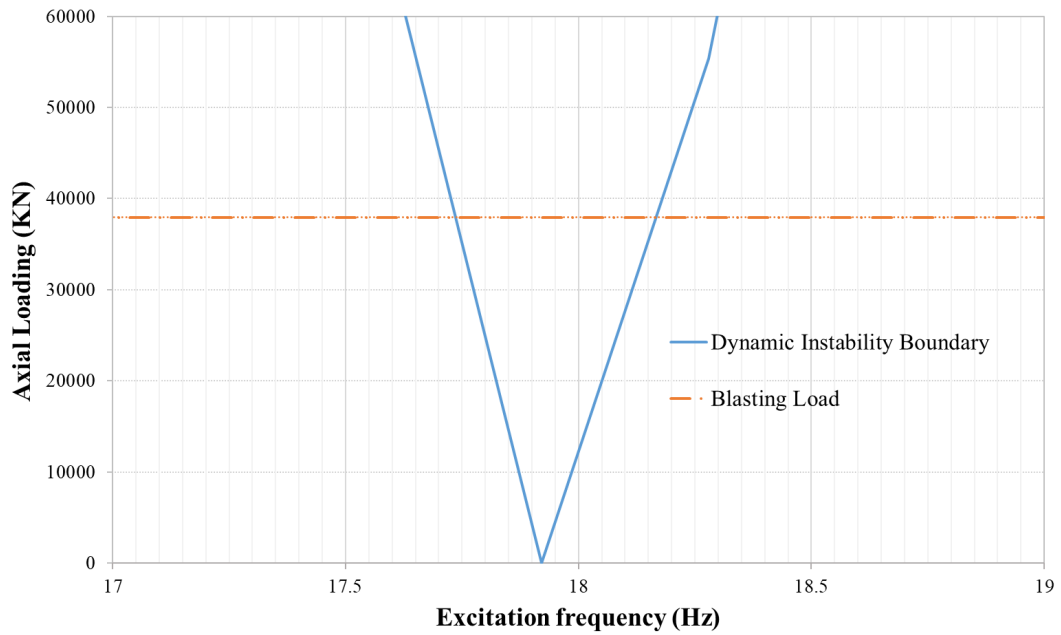


Figure 5.3: Dynamic buckling diagram of rock slope for blast loading

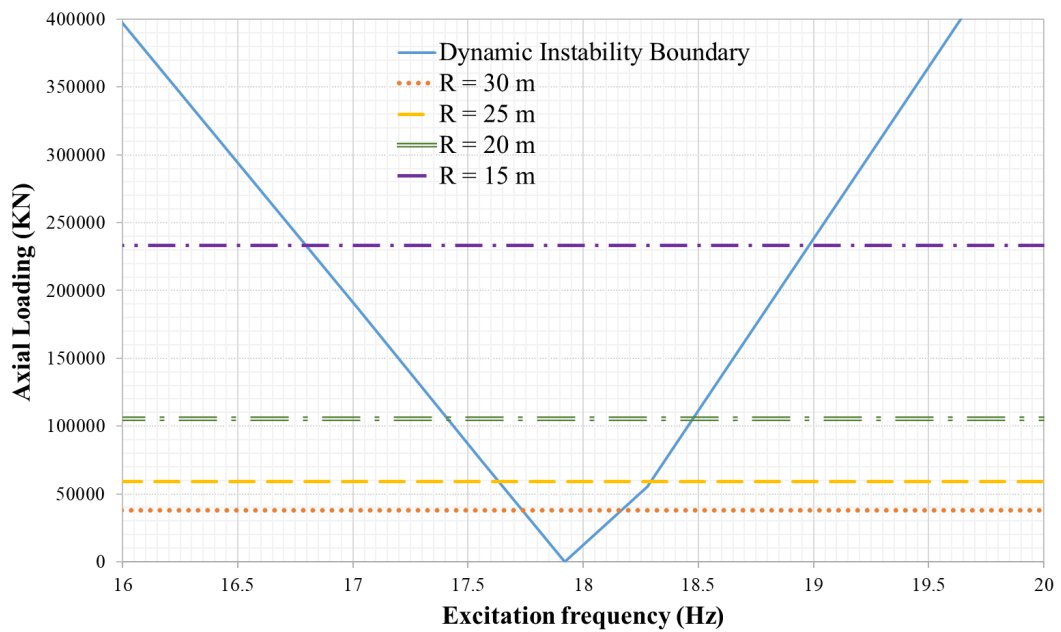


Figure 5.4: Blast loading at R = 30 m, 25 m, 20 m, 15 m.

The frequency of blasting vibrations ranges from 2 Hz - 50 Hz in most cases, the calculation average can be taken as 17.35 Hz. The waveform generated from the blasting will have high as well as low frequencies, wherein the high frequency can

be seen at the beginning where the peaks and troughs are close together in time, and low frequency at the end where the waves are further apart in time. The frequency below 20 Hz is considered as the low frequency which usually shakes the slopes, rocks, and buildings the most.

Therefore, a separate consideration should be made if the natural frequency of rock beam slope lies within the limit of 2-50 Hz, and dynamic stability assessment should be approached. Because even if a rock slope is statically stable and withstands the blasting load, it can be dynamically unstable due to the excitation frequencies, which may result in unexpected buckling and slope failure. The understanding of blasting vibration frequency and amplitude is essential to prevent unexpected collapse in the surrounding of blasting site.

5.6 Summary

The importance of dynamic stability assessment of rock slope against blasting vibration is clarified, and the equation of motion for the rock slope under dynamic excitation is derived. The dynamic instability regions for the rock slope are developed, and the effects of blasting distance are assessed. A risk of the dynamic instability increases for a given rock slope, with the decrease in distance to the origin of blasting.

Chapter 6

Dynamic Stability of Beams under Wind Loading

6.1 Introduction

Owing to the reports of failure of the beams under windstorm, Huang et al. (2014) considered the dynamic stability study of Euler beam under axially applied wind force. In their research, they solved the Mathieu- Hill equation for the dynamic stability under arbitrary loading based on the Floquet method. Huang transformed the arbitrary loading to the sinusoidal function prior to solving it. This chapter focuses on solving the dynamic stability of beams on elastic foundations under arbitrary loading.

The wind force data collected from the TJ-2 wind tunnel Tongji University were used for the case study (Zhou et al., 2011). Data were processed with proportional load strategy so that they could change the amplitude of excitation according to the specimen of the experiment. The sampling loading data are shown here as $a(t)$.

The wind load data shown in Fig. 6.1 has total samples of $N = 6000$, with sample recording frequency of $f_s = 9.58$ Hz, so that the total load duration is $t_{max} = 626.3$ s. The maximum recorded amplitude of wind sampling data is

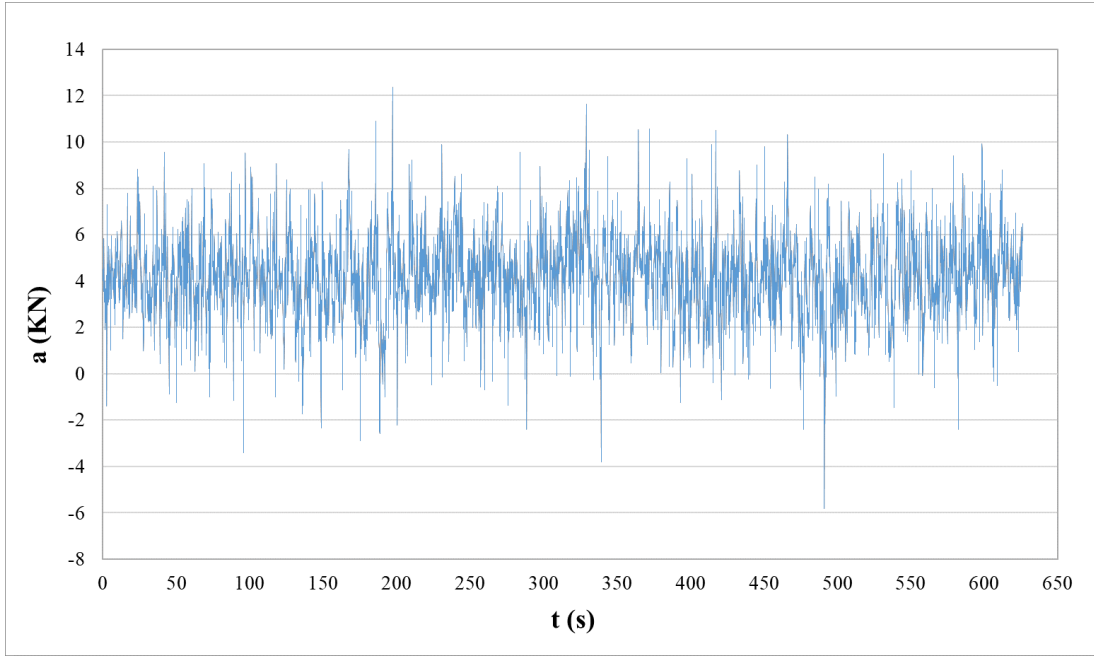


Figure 6.1: Wind sampling data

12,367 N, which was considered as relatively high and transformation of loading was conducted as follows,

$$a'(t) = \frac{a(t) - a_0}{\bar{a}}, \quad (6.1)$$

where $a'(t)$ is the based loading, $a_0 = 4190$ N is the mean amplitude and $\bar{a} = 288.87$ N is defined as the maximum harmonic amplitude. The plot of the new wind loading is shown in Fig. 6.2.

Moreover, the loading was taken in terms of,

$$a'(t) = \sum_{n=1}^{\infty} a'_n \cos(n\theta t). \quad (6.2)$$

Dynamic stability assessment of beams was conducted by solving Mathieu - Hill equation with eigenvalue problem to establish boundary conditions. In order to reduce the complexity in calculation only the first 100 readings, where the data for period $T = 10.44$ s was taken. Concisely, the method transforms the arbitrary loading through the Fourier series in order to assess the dynamic stability of Euler

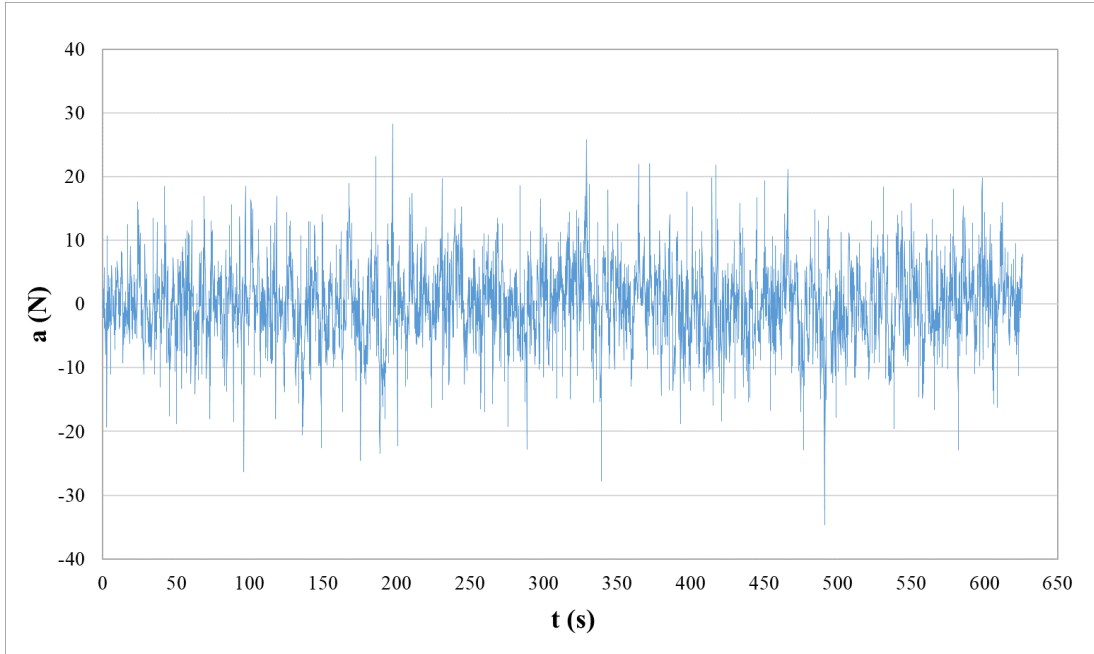


Figure 6.2: Modified wind sampling data

beam. However, Fourier series itself is a harmonic function, and the arbitrary values of sampling data were not processed directly for the dynamic stability assessment.

6.2 Solution using Pipes method

The solution for arbitrary loadings using Pipes method can be provided under certain conceptual assumptions. In order to evaluate dynamic stability of beams on elastic foundations for the sum of step loading, as mentioned in section 3.6, 4.2 & 4.3, a loading function $P(t)$ can be divided into δ number of step loadings as $H_1, H_2, \dots, H_\delta$ acting at constant period $T_0 = \frac{T}{\delta}$. These step loadings are constant values of loadings and have no relation with each other. Arbitrary loading as wind excitation or any sampling data is constantly measured value of loadings at uniform intervals, which can be substituted into the Hill equation as the step loadings. Hence, the dynamic stability assessment can be provided for wind loading, and the method can be illustrated with examples.

Example 1 Assessing dynamic stability of HEB 200 beam of length 7m under wind sampling data obtained in Fig. 6.1.

Here first thirty data ($N = 30$) is taken for ease of calculation, as shown in Fig. 6.3. However, any N number of data can be assessed for the dynamic stability of the beam. The natural frequency of the beam $\omega_n = \left(\frac{n\pi}{L}\right)^2 \sqrt{\frac{EI}{\rho A}} = 52.762$

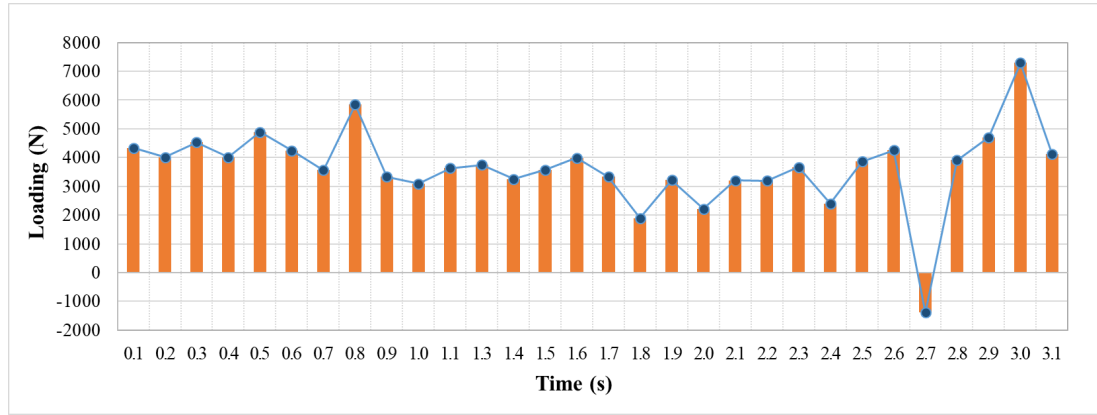


Figure 6.3: Wind sampling data, N=30

rad/s and the Euler critical loading $P_n = EI\left(\frac{n\pi}{L}\right)^2 = 847235$ N is calculated for $n = 1$. The frequency of wind sampling is $f_s = 9.58$ Hz, which gives the period of load excitation $T_0 = 0.1044$ s for the calculation. The calculation model is able to assess the dynamic stability of beam up to 847235 N of excitation loading. Loading greater than the Euler critical loading will statically buckle the beam.

Each sampling data will act as H_k for the calculation so that $N = 30$ will produce $H_1, H_2, H_3, \dots, H_{30}$. Following to the values of H_k , the matrix for dynamic stability condition can be derived from $[M] = [M]_{30} \cdot [M]_{29} \cdot [M]_{28} \cdot \dots \cdot [M]_1$. Table 6.1 shows the calculated values of P_k, Q_k and R_k from which multiplication of matrix can be computed as

$$[M] = \begin{bmatrix} A & B \\ C & D \end{bmatrix} = \begin{bmatrix} 0.03708346 & 0.018961376 \\ -52.6518663 & 0.044444877 \end{bmatrix}. \quad (6.3)$$

Table 6.1: Solution components for Example - 1

Step	H_k	g_k	ϕ_k	P_k	Q_k	R_k
1	4337.008	52.6268	5.4942	0.7046	-0.01348	37.3447
2	4008.147	52.6371	5.4953	0.7054	-0.01347	37.3122
3	4528.771	52.6208	5.4936	0.7041	-0.01349	37.3636
4	4008.147	52.6371	5.4953	0.7054	-0.01347	37.3122
5	4888.257	52.6096	5.4924	0.7033	-0.01351	37.3990
6	4242.843	52.6298	5.4945	0.7048	-0.01348	37.3354
7	3559.649	52.6511	5.4968	0.7064	-0.01344	37.2678
8	5845.930	52.5797	5.4893	0.7011	-0.01356	37.4930
9	3333.826	52.6581	5.4975	0.7069	-0.01343	37.2454
10	3093.120	52.6656	5.4983	0.7075	-0.01342	37.2215
11	3629.486	52.6489	5.4965	0.7062	-0.01345	37.2747
12	3749.123	52.6452	5.4962	0.7059	-0.01345	37.2866
13	3252.541	52.6607	5.4978	0.7071	-0.01343	37.2374
14	3575.391	52.6506	5.4967	0.7064	-0.01344	37.2694
15	3989.830	52.6377	5.4954	0.7054	-0.01347	37.3104
16	3335.543	52.6581	5.4975	0.7069	-0.01343	37.2456
17	1889.874	52.7031	5.5022	0.7102	-0.01336	37.1018
18	3220.199	52.6617	5.4979	0.7072	-0.01343	37.2342
19	2217.303	52.6929	5.5011	0.7095	-0.01337	37.1344
20	3209.895	52.6620	5.4979	0.7072	-0.01343	37.2331
21	3197.588	52.6624	5.4980	0.7072	-0.01343	37.2319
22	3666.121	52.6478	5.4964	0.7061	-0.01345	37.2784
23	2401.339	52.6872	5.5005	0.7091	-0.01338	37.1528
24	3859.029	52.6417	5.4958	0.7057	-0.01346	37.2974
25	4249.712	52.6295	5.4945	0.7048	-0.01348	37.3360
26	-1390.716	52.8053	5.5129	0.7177	-0.01319	36.7716
27	3906.827	52.6402	5.4956	0.7056	-0.01346	37.3022
28	4700.786	52.6155	5.4931	0.7038	-0.01350	37.3805
29	7297.324	52.5343	5.4846	0.6977	-0.01364	37.6346
30	4112.902	52.6338	5.4950	0.7051	-0.01347	37.3225

The dynamic stability condition can be assessed from the boundary condition given as

$$\left| A + D \right| = 0.081528 < 2, \quad \textit{Stable Vibration.} \quad (6.4)$$

So it can be said that, under provided wind loading, the beam will undergo stable vibrations.

Example 2 Assess the dynamic stability of the steel beam with dimensions 1000 mm x 50 mm x 9 mm, Modulus of elasticity $E = 2.1 \times 10^{11}$ N/m², resting on elastic foundation $k = 20$ kN/m² under excitation of wind sampling data shown in Fig. 6.3.

The fundamental frequency of the beam $\omega_n = \left(\frac{n\pi}{L}\right)^2 \sqrt{\frac{EI}{\rho A}} = 132.58$ rad/s, $\alpha = 1.322$ and natural frequency $\omega_m = 152.35$ rad/s can be calculated from Eq.(2.14) and Eq.(2.24). Moreover $\mu = 0.000120144$ can be obtained using Eq.(2.25).

The Euler critical loading $P_n = EI\left(\frac{n\pi}{L}\right)^2 = 6296$ N is computed. The elastic foundation provides support to the beam, which increase the buckling capacity of the beam. Therefore, this calculation model is capable of assessing dynamic stability of beams on elastic foundations till excitation loading is $H_k = \alpha P_n = 1.322 \times 6296 = 8323$ N. Table 6.2 shows the calculated value of P_k , Q_k and R_k .

Table 6.2: Solution components for Example - 2

Step	H_k	g_k	ϕ_k	P_k	Q_k	R_k
1	4337.008	105.4132	11.0051	0.0150	-0.00949	105.4014
2	4008.147	109.6752	11.4501	0.4441	-0.00817	98.2686
3	4528.771	102.8465	10.7372	-0.2504	-0.00941	99.5689
4	4008.147	109.6752	11.4501	0.4441	-0.00817	98.2686
5	4888.257	97.8536	10.2159	-0.6995	-0.00730	69.9327
6	4242.843	106.6510	11.1344	0.1437	-0.00928	105.5434
7	3559.649	115.2338	12.0304	0.8628	-0.00439	58.2609
8	5845.930	83.1012	8.6758	-0.7353	0.00816	-56.3256
9	3333.826	117.9335	12.3123	0.9694	-0.00208	28.9573
10	3093.120	120.7447	12.6057	0.9990	0.00038	-5.4988
11	3629.486	114.3860	11.9419	0.8147	-0.00507	66.3334
12	3749.123	112.9189	11.7887	0.7166	-0.00618	78.7576
13	3252.541	118.8903	12.4121	0.9890	-0.00124	17.5483
14	3575.391	115.0433	12.0105	0.8525	-0.00454	60.1285
15	3989.830	109.9077	11.4744	0.4657	-0.00805	97.2626
16	3335.543	117.9132	12.3101	0.9689	-0.00210	29.1946
17	1889.874	133.9154	13.9808	0.1490	0.00738	-132.4208
18	3220.199	119.2688	12.4517	0.9941	-0.00091	12.9275
19	2217.303	130.4632	13.6204	0.4883	0.00669	-113.8521
20	3209.895	119.3892	12.4642	0.9954	-0.00080	11.4476
21	3197.588	119.5328	12.4792	0.9967	-0.00068	9.6756
22	3666.121	113.9388	11.8952	0.7867	-0.00542	70.3369
23	2401.339	128.4820	13.4135	0.6572	0.00587	-96.8413
24	3859.029	111.5541	11.6462	0.6103	-0.00710	88.3740
25	4249.712	106.5612	11.1250	0.1345	-0.00930	105.5936
26	-1390.716	164.5540	17.1794	-0.0908	-0.00605	163.8745
27	3906.827	110.9553	11.5837	0.5595	-0.00747	91.9600
28	4700.786	100.4883	10.4910	-0.4789	-0.00874	88.2133
29	7297.324	53.4794	5.5832	0.7666	-0.01201	34.3379
30	4112.902	108.3358	11.3103	0.3148	-0.00876	102.8286

The boundary condition provides the important information about the dynamic stability of the beam resting on the elastic foundation under wind excitation, where matrix $[M]$ can be written as

$$[M] = \begin{bmatrix} A & B \\ C & D \end{bmatrix} = \begin{bmatrix} -0.031036546 & 0.022539595 \\ -47.4289489 & 2.224129476 \end{bmatrix}, \quad (6.5)$$

therefore, dynamic stability condition can be given as

$$\left|A + D\right| = 2.1930 > 2, \quad \textit{Unstable Vibration.} \quad (6.6)$$

Hence, it can be said that, under provided arbitrary loading, the beam on elastic foundations will undergo dynamically unstable vibrations.

However, unstable vibrations of the beam can be prevented by altering the geometric dimensions of the beam. Decreasing the length of the beam might be a more effective remedy as it also increases the Euler critical load. In this example, if the length of the beam reduces to 800mm, it starts to generate stable vibrations. Similarly, increasing the stiffness of foundation may also aid the stability of the beam, as stiffening the foundation to the $k = 23 \text{ kN/m}^2$ could lead to stable vibrations of the beam on elastic foundations.

The Pipes matrix method is able to assess the dynamic stability of beams resting on elastic foundations under any arbitrary loadings. The consideration should be made about a lengthiness of calculations, as it is required to create an individual matrix for each of the sampling data and at the end, multiplication of all individual matrix is also required to assess the dynamic stability. This model can also be employed for the seismic excitation.

6.3 Summary

The dynamic stability assessment of beams on elastic foundations under arbitrary loading using Pipes method is derived in this chapter. A small portion of sampling data is used as excitation for two systems (example 1 & example 2) for dynamic stability assessment. The results revealed that dynamic stability of beams under arbitrary excitations mostly depend upon the Euler Buckling load of the beams

and stiffness of the foundations.

Chapter 7

Conclusions

7.1 Summary of thesis achievements

The dynamic stability of axially loaded beams on the elastic foundations is systematically investigated in this thesis. The excitation is assumed to be various periodical loadings, and the arbitrary loading is also incorporated. The Pipes matrix method is used for assessing the dynamic stability of the beams on the elastic foundations. The dynamic stability diagrams are also obtained for various cases using numerical analysis, and multiple examples are also presented.

- The force equilibrium for infinitesimal column resting on the elastic foundation (Winkler) can generate the equation of motion of the system. Damping modification transforms the equation of motion into the Hill equation. Using Pipes matrix method, dynamic stability assessment for various periodic loading cases can be adequately determined. The dynamic instability regions are developed for the pulsating force using the numerical analysis.
- Parametric study of a beam on an elastic foundations for change in stiffness of foundation states that, the dynamic instability regions of the system will reduce in the area if the stiffness of supporting foundation increases.

- The principle dynamic instability regions shift towards a small ratio of frequencies (left) with elevation in the static load component.
- Any periodical loading can be assessed for the dynamic stability of beams on elastic foundations by merely transforming it into step loadings at equal intervals.
- The comparison results of Pipes method with Floquet theory and finite element method provides an idea about the accuracy of the Pipes matrix method for dynamic stability assessment, and it can be said that the solution obtained with the Pipes method is reliable and accurate.
- The statically stable rockslope under the excitation of blasting can be collapsed if blasting vibrations propagate with certain specific frequency, which can be obtained from the dynamic instability region of rock slope.
- The Pipes matrix method is also capable of providing the assessment of dynamic stability for arbitrary loading. However, the tediousness of the calculation largely depends upon the number of sampling data.

7.1.1 Assumptions and applications

Dynamic stability study for the arbitrary loading (wind loading) is carried out based on a assumption that loading has a periodic form, realistically arbitrary loading or wind excitation cannot be periodic. The elastic foundation for rock-slope study is assumed to be Winkler. However, more practical results can be obtained by assuming it as Pasternak type elastic foundation.

This advancement in the method of assessing dynamic stability can be accessed into many applications such as the dynamic stability of pile foundation and bridge column under earthquake vibration, the dynamic stability of rock slope

against the blasting vibrations, the steel column under machine vibration in industrial buildings, bridge deck stability against wind loading, harbour deck stability against the wave excitation.

7.2 Future scope

Some of the future research areas in the field of dynamic stability assessment for a beam on elastic foundations are described below:

- As Floquet theory is validated with experimental results(Bolotin, 1964; Svensson, 2001; Mohanty et al., 2012) and comparison results of the Pipes method is proven to be identical with Floquet theory and finite element method. However, experimental results and comparison results for the arbitrary solution has not been obtained yet. So the experimental work for validating the results for arbitrary loading should be carried out. Experimental set up from Svensson (1996) can be adapted, replacing transverse constraints by springs with known stiffness for the experimental study of beams on elastic foundations under various excitations.
- The foundation is considered uniform throughout the length of the beam, which can be considered as variable foundation and solutions can be provided for dynamic stability.
- The recent model is capable of processing arbitrary loading, and sampling data from wind loadings and earthquake loadings, however the primary data for earthquake loadings are usually in the form of ground accelerations. So modification in the modeling should be made to process ground acceleration data.

Bibliography

- Abbas, B. and Thomas, J. (1978). Dynamic stability of timoshenko beams resting on elastic foundation. *Journal of Sound and Vibration*, 60:33–44.
- Ahuja, R. and Duffield, R. (1975). Parametric instability of variable cross section beams resting on an elastic foundation. *Journal of Sound and Vibration*, 39:159–174.
- Alazzawi, A. (2017). Free vibration of simply supported beam on elastic foundations. *Al-Nahrain Journal for Engineering Sciences*, 20:353–357.
- Arduino, P., McGann, C., Ghofrani, A., et al. (2017). Numerical evaluation of forces on piled bridge foundations in laterally spreading soil. Technical report, Washington (State). Dept. of Transportation. Research Office.
- Beliaev, N. M. (1924). Stability of prismatic rods subjected to variable longitudinal forces. *Collection of Papers: Enineering Constructions and Structural Mechanics*, pages 149–167.
- Bittanti, S. and Colaneri, P. (2009). *Periodic Systems- Filtering and Control*, volume 1. Springer, Milan.
- Bolotin, V. V. (1964). *The dynamic stability of elastic systems*. Holden- Day, Inc., San Francisco.

- Briseghella, L., Majorana, C. E., and Pellegrino, C. (1998). Dynamic stability of elastic structure: a finite element approach. *Computers and structures*, 69:11–25.
- Brown, J. E., Hutt, J. M., and Salama, A. E. (1968). Finite element solution to dynamic stability of bars. *AIAA Journal*, 6:1423–1425.
- Burney, S. and Jaeger, L. (1971). A method of determining the region of instability of a column by a numerical method approach. *Journal of Sound and Vibration*, 15:75–91.
- Cavers, D. (1981). Simple methods to analyze buckling of rock slopes. *Rock mechanics*, 14(2):87–104.
- Chen, M., Lu, W., Yan, P., and Zhou, C. (2013). New method for dynamic stability analysis of rock slope under blasting vibration based on equivalent acceleration and sarma method. *Canadian Geotechnical Journal*, 51(4):441–448.
- Deng, J., Gong, Y., Elsheikh, T., and Patel, B. (2019). On the mechanism of pillar rockbursts induced by dynamic disturbances from blasting. *The 14th International Congress on Rock Mechanics and Rock Engineering (ISRM 2019)*, September 13 - 18, Brazil. (accepted).
- Deng, J. and Gu, D. (2018). Buckling mechanism of pillar rockbursts in underground hard rock mining. *Geomechanics and Geoengineering*, 13(3):168–183.
- Dowding, C. and Gilbert, C. (1988). Dynamic stability of rock slopes and high frequency traveling waves. *Journal of Geotechnical and Geoenvironmental Engineering - ASCE*, 114(10):1069–1088.
- Eisenberger, M. and Clastronik, J. (1987). Vibration and buckling of a beam on a

- variable winkler elastic foundation. *Journal of Sound and Vibration*, 115:233–241.
- Engel, R. S. (1991). Dynamic stability of an axially loaded beam on an elastic foundation with damping. *Journal of Sound and Vibration*, 146:463–477.
- Hu, X.-Q. and Cruden, D. (1993). Buckling deformation in the highwood pass, alberta, canada. *Canadian Geotechnical Journal*, 30(2):276–286.
- Hu, Y. and Kempfert, H. (1999). The buckling failure of tunnels induced by high horizontal stress in jointed rocks. In *Numerical models in geomechanics. Proc. of the 7th international symposium, Graz, September*, pages 347–351.
- Huang, Y., Liu, A., Pi, Y., Lu, H., and Gao, W. (2017). Assessment of lateral dynamic instability of columns under an arbitrary periodic axial load owing to parametric resonance. *Journal of Sound and Vibration*, 395:272–293.
- Huang, Y.-Q., Lu, H.-W., Fu, J.-Y., Liu, A.-R., and Gu, M. (2014). Dynamic stability of euler beams under axial unsteady wind force. *Mathematical Problems in Engineering*, vol. 2014, Article ID 434868:1–22.
- Iwastubo, T., Saigo, M., and Sugiyama, Y. (1973). Parametric instability of clamped – clamped and clamped – simply supported columns under periodic axial load. *Journal of Sound and Vibrations*, 30:65–77.
- Kerr, A. D. (1964). Elastic and viscoelastic foundation models. *Journal of Applied Mechanics*, 31(3):491–498.
- Krylov, N. and Bogoliubov, N. (1935). An investigation of the appearance of resonance of the transverse vibrations of rods due to the action of normal periodic forces on an end. *Collection of Papers: Investigation of Vibration of Structures*, pages 25–42.

- Machado, S., Filipich, C., and Cortinez, V. (2007). Parametric vibration of thin walled composite beam with shear deformation. *Journal of Sound and Vibration*, 305:563–581.
- Mills, C. (1987). The design of concrete structure to resist explosions and weapon effects. In *Proceeding of the 1st international Conference on Concrete for Hazard Protection*, pages 61–73.
- Mohanty, S., Dash, R. R., and Rout, T. (2012). Static dynamic stability analysis of a functionally graded timoshenko beam. *International Journal of Structural Stability and Dynamics*, 12(04):1–33.
- Mohanty, S. C. (2007). Parametric instability of pretwisted cantiliver beam with the localised damage. *International Journal of Acoustic and Vibration*, 12:153–161.
- Mohanty, S. C., Dash, R. R., and Rout, T. (2011). Parametric instability of functionally graded timoshenko beam on winkler’s elastic foundation. *Nuclear Engineering and Design*, 241:2698–2715.
- Newmark, N. and Hansen, R. (1961). Design of blast resistant structures. *Shock and vibration handbook*, vol. 3, McGraw-Hill, New York, USA.
- Nilsen, B. et al. (1987). Flexural buckling of hard rock-a potential failure mode in high rock slopes? In *6th ISRM Congress*. International Society for Rock Mechanics.
- Pipes, L. A. (1953). Matrix solution of equations of the mathieu-hill type. *Journal of applied physics*, 24(7):902–910.
- Pipes, L. A. (1964). The dynamic stability of a uniform straight column excited by pulsating load. *Journal of Franklin Institute*, 227:534–551.

- Pipes, L. A. and Harvill, L. R. (2014). *Applied mathematics for engineers and physicists*. Courier Corporation.
- Qi, S., Lan, H., and Dong, J. (2015). An analytical solution to slip buckling slope failure triggered by earthquake. *Engineering Geology*, 194:4–11.
- Saha, K., Kar, R., and Datta, P. (1997). Dynamic stability of a rectangular plate on non-homogeneous winkler foundation. *Computers & structures*, 63(6):1213–1222.
- Shastry, B. and Rao, G. (1987a). Stability boundaries of a cantiliver column subjected to an intermediate periodic concentrated axial load. *Journal of Sound and Vibration*, 116:195–198.
- Shastry, B. P. and Rao, G. V. (1987b). Dynamic stability od cantilever column with an intermediate concentrated periodic load. *Journal of Sound and Vibration*, 113:194–197.
- Stevens, K. K. and Evan-Iwanowski, R. M. (1969). Parametric resonance of viscoelastic column. *International Journal of Solid and Structures*, 5:755–761.
- Sun, Q., Lu, Q., and Wu, J. (2011). Methods of dynamic stability critical load of foundation pile. In *2011 International Conference on Electric Technology and Civil Engineering (ICETCE)*, pages 6690–6693.
- Svensson, I. (1996). Dynamic buckling of a beam with transverse constraints. *Nonlinear Dynamics*, 11:315–328.
- Svensson, I. (2001). Dynamic instability regions in a damped system. *Journal of Sound and Vibration*, 244:779–793.
- Tommasi, P., Verrucci, L., Campedel, P., Veronese, L., Pettinelli, E., and Ribacchi, R. (2009). Buckling of high natural slopes: the case of lavini di marco (trento-italy). *Engineering Geology*, 109(2):93–108.

- Xie, W.-C. (2006). *Dynamic stability of structures*. Cambridge University Press.
- Yokoyama, T. (1988). Parametric instability of timoshenko beams resting on an elastic foundation. *Computers and Structures*, 28:207–216.
- Zhou, X., Huang, P., Gu, M., and Mi, F. (2011). Wind loads and responses of two neighboring dry coal sheds. *Advances in structural engineering*, 14(2):207–221.
- Zhou, Y. and Zhao, J. (2011). *Advances in rock dynamics and applications*. CRC Press.

Appendix A

Calculation Procedures

The calculations for assessing dynamic stability regions are done with the MS Excel software, for the sake of ease in keeping data in tabular format for separate input and output. The screen captures of excel sheets represent the format of calculations.

The calculation data for the pulsating force is shown in Fig. A.1.

H	γ	P	$ r $	plot H	Plot γ
5	0.97	100			
10	0.97	100			
15	0.97	100			
20	0.97	100			
25	0.97	100	0.99961		
30	0.97	100	0.99971		
35	0.97	100	0.99983		
40	0.97	100	0.99996		
45	0.97	100	1.00011	45	0.97
50	0.97	100	1.00028	50	0.97
55	0.97	100	1.00047	55	0.97
60	0.97	100	1.00068	60	0.97
65	0.97	100	1.0009	65	0.97
70	0.97	100	1.00114	70	0.97
75	0.97	100	1.0014	75	0.97
80	0.97	100	1.00168	80	0.97
85	0.97	100	1.00197	85	0.97
90	0.97	100	1.00229	90	0.97

Figure A.1: Calculation sheet for pulsating force

In Fig. A.1, H is dynamic load component, γ ratio of frequencies, P static load

